

Marshall University
Marshall Digital Scholar

Theses, Dissertations and Capstones

2002

Pyridoimidazolium Cationic Dyes: Theory, Synthesis, and Sub-cellular Localization

Robert William Rambacher

Follow this and additional works at: <http://mds.marshall.edu/etd>



Part of the [Organic Chemistry Commons](#)

Recommended Citation

Rambacher, Robert William, "Pyridoimidazolium Cationic Dyes: Theory, Synthesis, and Sub-cellular Localization" (2002). *Theses, Dissertations and Capstones*. Paper 806.

This Thesis is brought to you for free and open access by Marshall Digital Scholar. It has been accepted for inclusion in Theses, Dissertations and Capstones by an authorized administrator of Marshall Digital Scholar. For more information, please contact zhangj@marshall.edu.

**Pyridoimidazolium Cationic Dyes:
Theory, Synthesis, and Sub-cellular Localization**

A Thesis Presented to
the Graduate College of
Marshall University

In Partial Fulfillment
of the Requirements for the Degree of
Masters of Science
Chemistry

By
Robert William Rambacher

Marshall University
Huntington, West Virginia
December, 2002

This thesis was accepted on October 20, 2002 as meeting the research requirements for the Master's Degree.

Dr. Robert J. Morgan, Ph.D
Thesis Committee Chair

Dr. Michael L. Norton, Ph.D.
Thesis Committee Member

Dr. Lawrence R. Schmitz, Ph.D
Thesis Committee Member

Abstract
Pyridoimidazolium Cationic Dyes: Theory, Synthesis, and Sub-cellular Localization

by: Robert William Rambacher

(PICs, Figure 1) are a new class of fluorescent dyes which are prepared by an exceedingly flexible methodology. Using computational chemical methods, the excitation and emission maxima of these dyes were simulated. This was best accomplished through geometry optimization (MM+) followed by calculating the electronic spectrum with ZINDO/S. This protocol has been found to be effective and has the potential to greatly streamline the design of new longer wavelength dyes. Several new longer wavelength dyes have now been identified as synthetic targets.

The presence of amino groups on a known fluorescent ring system is well established to markedly affect the optical properties of the dye. Methodology had been developed toward the amination of different position on the 2-(2-pyridyl)-carboxyl-quinoline ring system, leading to the testing of 3 new amino substituted fluorescent dyes, including 4-amino-2-(2-pyridyl)-quinoline. This is also the precursor to 4-isothiocyanato-2-(2-pyridyl)-quinoline, which is a potentially useful cellular tag for proteins.

The behavior of green fluorescent PICs in live smooth muscle cells was probed using confocal microscopy. Several dyes were proven to be effective in staining the mitochondria. A novel red (488/675nm) nuclear envelope stain was identified and investigated.

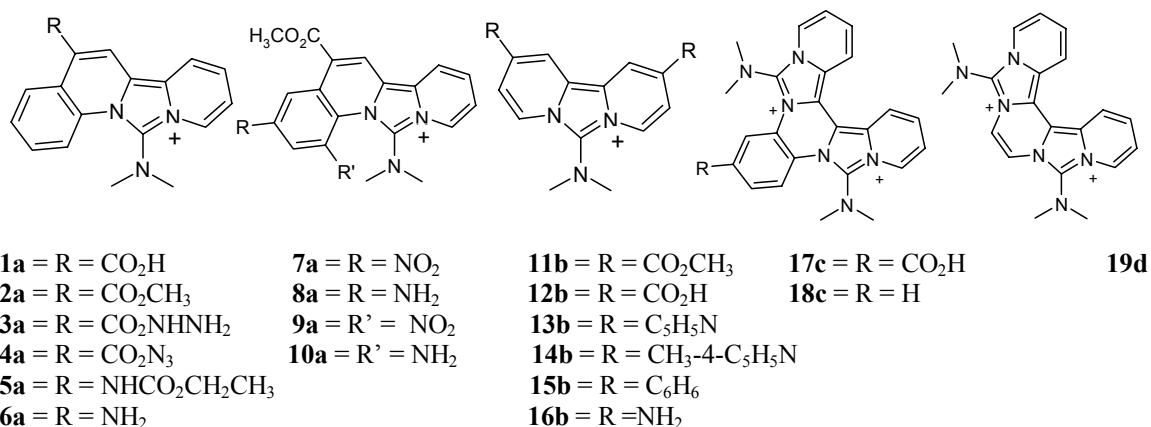


Figure 1: PICs investigated in research

Acknowledgments

I would like to thank Dr. Norton for his general advice and, who during the SEM class, spawned part of my thesis. I would also like to thank Dr. Wright whose students, Ava Dykes and Chenwei Lee, supplied cells. Thanks to Dr. Frankberry and the rest of the biology department for all their help and use of their facilities. Also I would like to thank my thesis committee and the rest of the Chemistry Department. Lastly, a special thank you to Dr. Morgan for his expert tutelage in all matters.

Table of Contents

Abstract.....	iii
Acknowledgments.....	iv
Table of Contents.....	v
List of Figures.....	vi
List of Tables.....	viii
 Chapter 1: Theory of Dyes	
Introduction.....	1
Results.....	9
Experimental.....	14
Conclusion.....	15
 Chapter 2: Dyes	
Introduction.....	16
Experimental.....	20
Results.....	30
Conclusion.....	32
 Chapter 3: Confocal Microscopy	
Introduction.....	33
Experimental.....	42
Results.....	42
Conclusion.....	53
 Chapter 4: Summary and Conclusion.....	54
 Bibliography.....	56
Appendix I.....	57

List of Figures

Figure 1: The Jablonski diagram	1
Figure 2: Stokes's shift	2
Figure 3: PICs investigated in research	3
Figure 4: Structures of coumanins	6
Figure 5: Excitation and emission maxima for PICs 1b.....	10
Figure 6: Actual excitation compared to theoretical excitation maximum....	11
Figure 7: Actual emission compared to theoretical emission maximum.....	13
Figure 8: A representation of the shoulder on the 77 K data.....	13
Figure 9: Literature Scheme.....	17
Figure 10: Scheme used to synthesis amino PICs	18
Figure 11: Synthesis of Amino-ester PICs.....	20
Figure 12: ^1H 500 MHz NMR of 4-carbohydrazido-2-(2-pyridyl)quinoline..	21
Figure 13: $^1\text{H}^1\text{H}$ COSY 500 MHz NMR of Figure 12.....	22
Figure 14: ^1H 500 MHz NMR of 4-ethylcarbamato-2-(2-pyridyl)quinoline..	24
Figure 15: $^1\text{H}^1\text{H}$ COSY 500 MHz NMR of Figure 14.....	24
Figure 16: ^1H 500 MHz NMR of 4-amino-2-(2-pyridyl)quinoline.....	25
Figure 17: $^1\text{H}^1\text{H}$ COSY 500 MHz NMR of Figure 16.....	27
Figure 18: ^1H 500 MHz NMR of nitro isomers.....	27
Figure 19: $^1\text{H}^1\text{H}$ COSY 500 MHz NMR of nitro isomers.....	28
Figure 20: ^1H 500 MHz NMR of amino ester compound.....	29
Figure 21: $^1\text{H}^1\text{H}$ COSY 500 MHz NMR of amino ester compound.....	29
Figure 22: Base structures for assignment by ^1H COSY	31
Figure 23: Base Structures of the assignment of the isomer mixtures.....	32
Figure 24: How a Confocal Microscope works?.....	33
Figure 25: Optical filters for the Confocal Microscope	36
Figure 26: Rhodamine 123.....	37
Figure 27: ER-Tracker Blue white DPX	37
Figure 28: MitoTracker Red CM- H_2Xros	38
Figure 29: Live bovine pulmonary artery endothelial cells stained	38
Figure 30: BODIPY-ceramide derivatives.....	39
Figure 31: NBD-ceramide	39
Figure 32: Carbocyanine dyes	40
Figure 33: Dihydrorhodamine 123.....	40
Figure 34: Alexa Fluor 488 phalloidin	40
Figure 35: DAPI	41
Figure 36: MitroTracker red in smooth muscle cells of a rat's aorta.....	43
Figure 37: Dye 1a in smooth muscle cells of a rat's aorta.....	44
Figure 38: Dye 1a & MitoTracker in smooth muscle cells of a rat's aorta...	45
Figure 39: Dye 2a in smooth muscle cells of a rat's aorta	46
Figure 40: Dye 2a & MitoTracker in smooth muscle cells of a rat's aorta....	47
Figure 41: Dye 6a in smooth muscle cells of a rat's aorta.....	47
Figure 42: Dye 6a & MitoTracker in smooth muscle cells of a rat's aorta...	48
Figure 43: Dye 11b in smooth muscle cells of a rat's aorta	49
Figure 44: Dye 11b & MitoTracker in smooth muscle cells of a rat's aorta.	49

Figure 45: Dye 14b in smooth muscle cells of a rat's aorta.....	50
Figure 46: Dye 14b in smooth muscle cells of a rat's aorta.....	52
Figure 47: Dye 13b in smooth muscle cells of a rat's aorta.....	52

List of Tables

Table 1: Experimental and calculated absorption maximum.....	7
Table 2: Experimental and Calculated fluorescence maxima.....	8
Table 3: Excitation maximum of each dye	10
Table 4: Theoretical and actual emission maximum.....	12
Table 5: Parameter for semi-empirical methods	14
Table 6: Sub-cellular co-localization vector for targeted organelle.....	41

Chapter 1: Theory of Dyes

Introduction

Fluorescence is a phenomenon during which a molecule absorbs a photon, is raised to a high-energy state, where it remains for sometime, then returns to the ground state, emitting a photon of light. While in the high-energy state the molecule undergoes an internal conversion, which is the radiationless transition between energy states of the same spin. In a molecular system, the energy required to excite an electron into a higher energy state is always greater than the emission energy. The Jablonski diagram (Figure 1) indicates how fluorescence and phosphorescence can be produced. The difference in the excitation and the emission maxima is called the Stoke's shift (Figure 2).

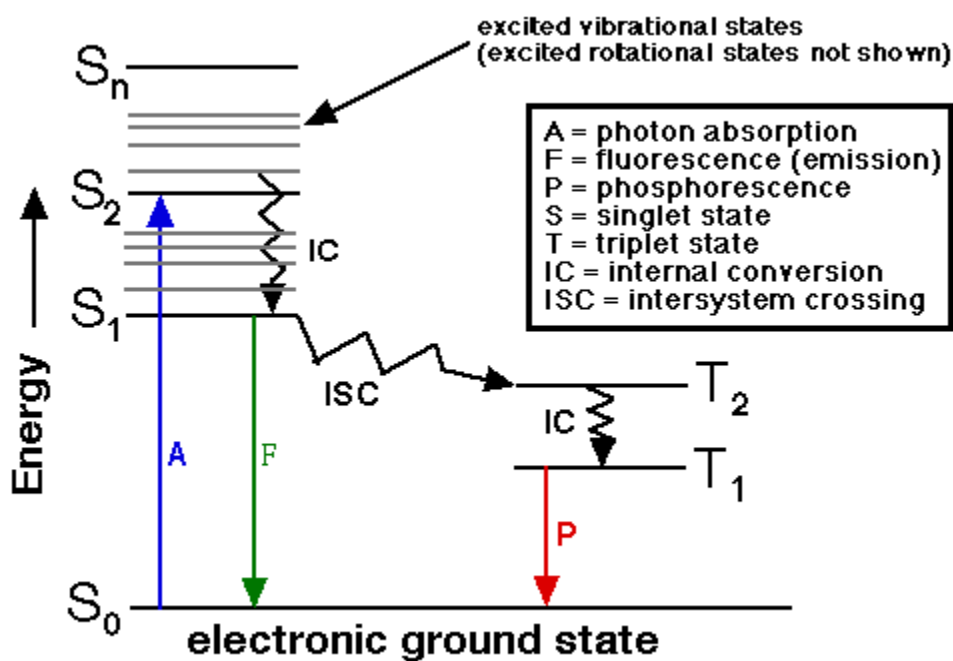


Figure 1: The Jablonski diagram

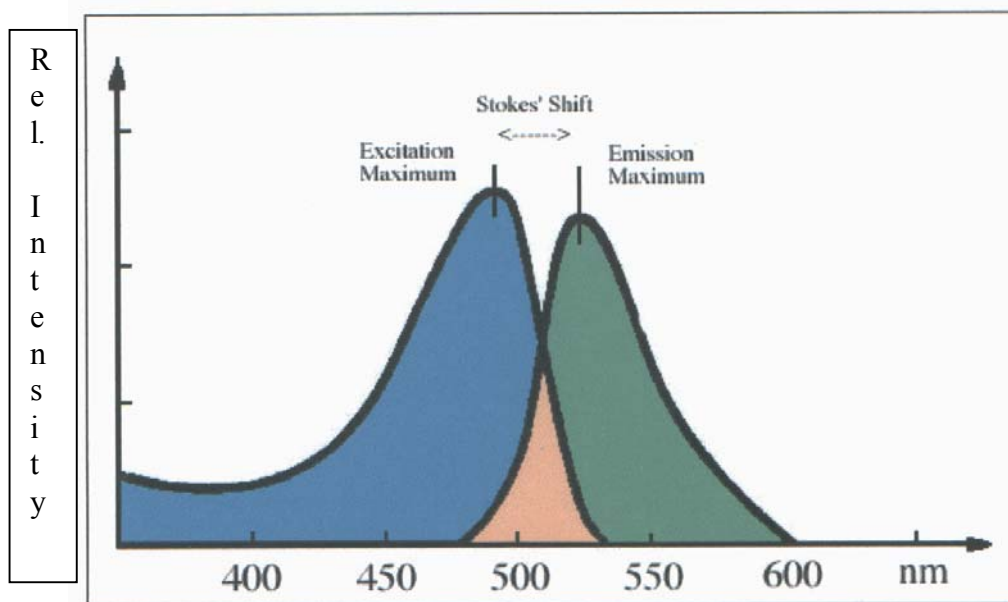


Figure 2: Stokes' shift, which is the difference between excitation and emission maxima

Considering the increasing importance and number of applications for fluorescent dyes in analytical,¹ medicinal,² and biochemical³ fields, there is a demand for more specific dyes and sensors, tailored to each application. A tremendous number of pyridoimidazolium cations (PICs, Figure 3) can be synthesized using our patented approach.¹ Molecular modeling might be a convenient and effective means of identifying dyes, which would show interesting optical properties, most notably, longer wavelength fluorescence. Computational chemistry is able to predict the structures, electronic spectra and other chemical properties of molecules with ample accuracy.⁴ There is a literature precedent suggesting that computer modeling offers a more systematic approach to the design of fluorescent dyes.⁶

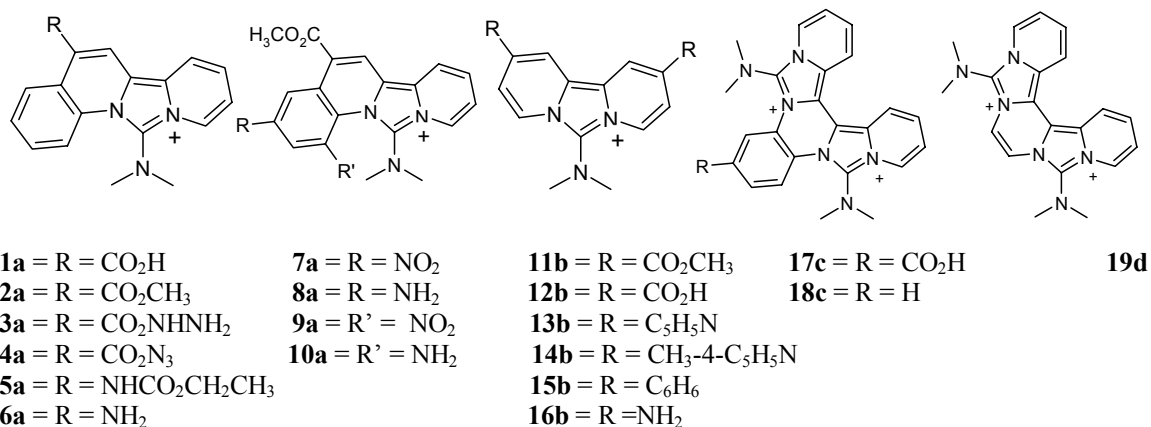


Figure 3: PICs investigated in research

Molecular modeling can be performed using either a semi-empirical or an *ab initio* approach. The semi-empirical methods are used more frequently by practical chemists than the more expensive and complicated *ab initio* methods for the prediction of molecular properties.⁴ Semi-empirical methods use parameters derived from experimental data, simplifying the approximation of the Schrodinger equation, and thus lowering the expense of the calculation. Semi-empirical calculations are reasonably accurate, can be obtained quickly, and can be applied to large or complex problems.

Many problems are simply not amenable to *ab initio* calculations because of their complexity, even when they are reduced to a minimum. For this reason semi-empirical methods were used for optimization (MM+) in this thesis. The optimization is an important element since overlooking small errors in the optimization will result in non-reliable calculations.⁴

Electronic spectra can be predicted by using molecular modeling to study excited states. There is little theoretical data on excited states available in the current literature.⁵

Modeling excited states and predicting the optical properties of molecules remains a difficult problem, due to the fact sometimes vibration states are ignored. Configuration interaction (CI) can be used to model excited states as combinations of single substitutions of the Hartree-Fock ground state.⁴ This method (Configuration Interaction-singles) is described by its founders as an “adequate zeroth-order treatment of excited states of molecules.”⁴ CI was used to determine the absorption and fluorescence spectral properties of pyridyl-quinoline derivatives with different substitution patterns. Experimental results were complemented by theoretical calculations using semi-empirical CI molecular orbital calculations (ZINDO/S), to aid in the design of new and longer wavelength absorbing and emitting dyes.

Coumarins⁶ (Figure 4) are a naturally occurring and easily synthesized family of fluorescent heterocycles. They have found widespread use as photosensitizers⁷ and laser dyes.^{8,9,10,11} Coumarins can be used to evaluate computational methodologies for the prediction of optical properties of dyes because a large amount of experimental results exist in the literature. This methodology from literature was used to study coumarins and was successful in predicting optical spectra. Fabian's⁶ group determined the optical properties of these coumarins as compared to known values and was not repeated during my research. This methodology allowed for the determination of the optical properties of new coumarins before synthesis.

Table 1 summarizes the excitation data obtained by the Fabian⁶ and the Zindo/s data. The electronic excitation energy is relatively insensitive to substitution. An

adequate correlation exists (Table 1) between the calculated and experimentally determined excitation energies (error of 0 to 3%) and the calculation of the emission energies (error of 0 to 7%) (Table 2). Low level *ab initio* calculations were also performed, but were less effective in modeling the electronic spectra than the combination of optimization with AM1 followed by electronic spectra simulation using ZINDO/S. The authors of the coumarin study were confident that higher levels of theory would not alter the present results, since low level *ab initio* were shown to be less effective than the semi-empirical methods. Substitution effects appear to exert a more pronounced effect on emission energies than on absorption energies.¹⁰

In Fabian⁶ work, the excitation and emission maxima were determined with geometry optimization with AM1, followed by calculation of the transition energies using ZINDO/S. The proper treatment of the effect of hydrogen bonding is outside the scope of this approximation. Solvents were shown to have very little effect on transition energy (100 cm⁻¹).

Computational methods allow the prediction of both absorption and emission maxima with reasonable accuracy (error 0 to 7 %) in the coumarin study. This methodology should also be effective in predicting the optical properties of PICs (pyridoimidazolium cations) with ample accuracy, due to the fact of the similarity of coumarins structure as compared to PICs. Thus, these calculations provide a valuable tool in the rational design of dyes with longer wavelengths like these developed in our laboratory.

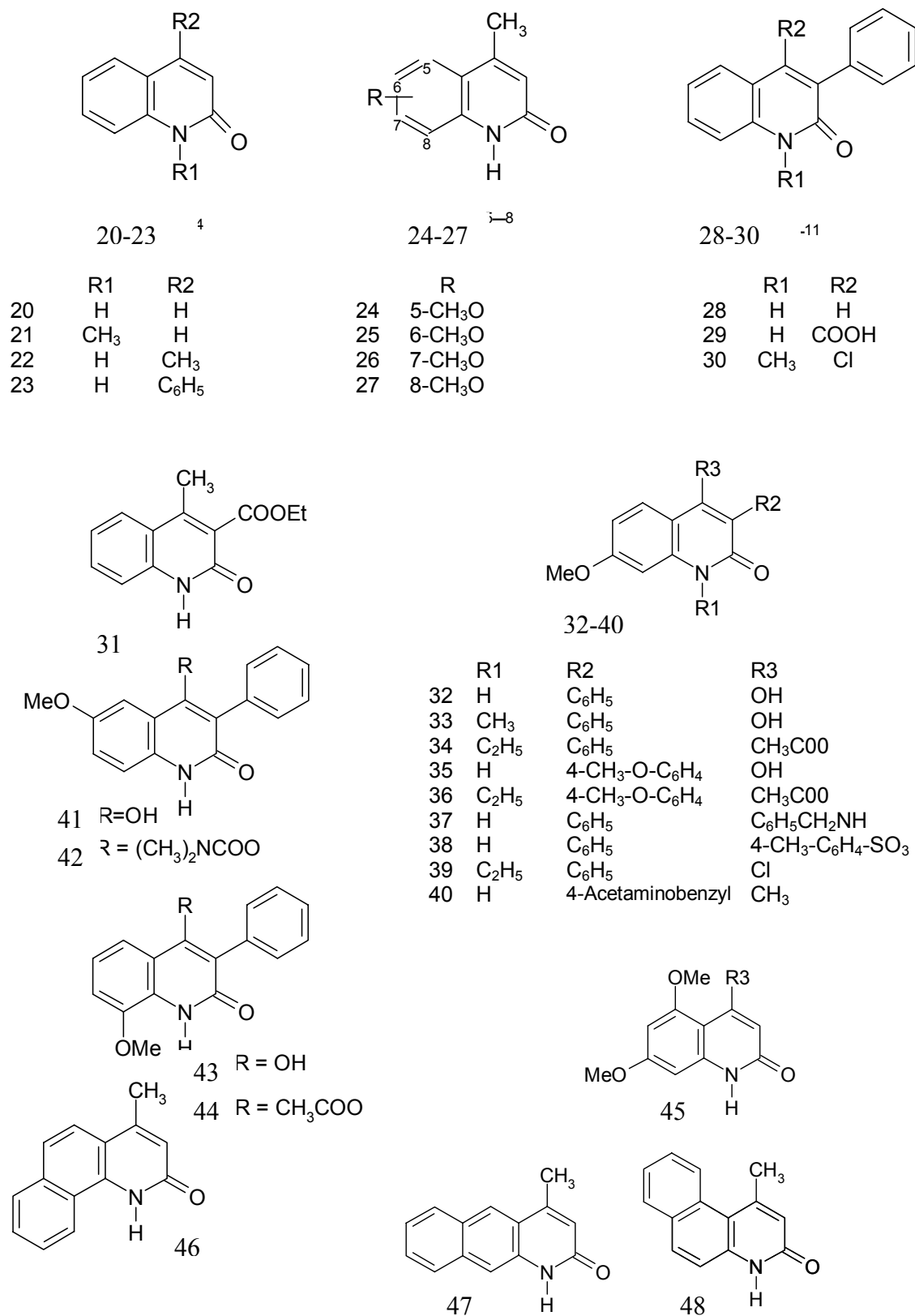


Figure 4: Structures of coumarins

Table 1¹⁰: Experimental and calculated (ZINDO) absorption maxima (cm^{-1}) extinction coefficients ϵ (1 mol^{-1}) and oscillator strength f

Table 1	Experimental and calculated (ZINDO) absorption maximum, extinction coefficient, and oscillator strengths			
Compd	$\nu_{\text{exp}} (\text{cm}^{-1})$	$\epsilon (1 \text{ mol}^{-1} \text{ cm}^{-1})$	$\nu_{\text{cal}} (\text{cm}^{-1})$	f
1	30000	3660	31300	0.174
2	29900	4250	31200	0.168
3	30200	6510	31700	0.154
4	29700	5940	31800	0.146
5	--	--	31200	0.084
6	28300	6550	28500	0.158
7	29200	10000	--	--
	30500	12900	31000	0.358
8	29500	3730	29900	0.05
9	29000	7850	30000	0.511
10	29100	6580	30300	0.432
11	29100	8390	29800	0.354
12	29800	6660	30900	0.195
13	30200	14400	29100	0.761
14	30000	14500	29100	0.704
15	29700	16900	29000	0.648
16	30000	17300	29100	0.781
17	29300	19300	28600	0.677
18	30300	10800	30100	0.48
19	30100	23400	29600	0.629
20	29500	16300	29200	0.611
21	29000	13000	--	--
	30300	17400	30800	0.396
22	28500	8070	27800	0.291
23	27900	9370	28400	0.254
24	30200	5750	29200	0.146
25	28900	5350	29300	0.153
26	30100	7230	--	--
	31300	10200	31300	0.334
	32700	10800	31600	0.162
27	26700	6400		
	28000	7200	28700	0.17
	29300	4600		
28	--	--	28100	0.043
29	--	--	28400	0.248

Table 2¹⁰: Experimental and calculated fluorescence maxima and quantum yield Φ_F

Table 2	Experimental and Calculated (ν^{exe} and ν^{c10}) fluorescence maxima and quantum yield Φ_F			
Compd	ν_F (cm ⁻¹)	Φ_F	ν^{exc} (cm ⁻¹)	ν^{c10} (cm ⁻¹)
1	26400	0.02	25900	31400
2	26300	0.01	29000	30600
3	26700	0.02	27500	31700
4	25100	0.01	27500	30300
	26500			
5				30700
6	24700	0.033	25400	27300
7	27200	0.052	28800	30800
	29300			
8	25400	0.009	26700	29400
	26400			
9	24400	0.061	26300	
	25600			
10	26100	0.011	23400	
	27300			
11	24000	0.018	23100	
	26000			
12	23300	0.01	27300	29500
	26800			
13	26500	0.009	21500	28300
14	26600	0.008	20800	
15	25500	0.105	24400	
16	25500	0.015		
	26300			
17	25100	0.028	21400	
18	26200	0.005		
19	26400	0.009		
20	25600	0.004	22200	25700
21	27000	0.051	28200	
22	24400	0.04		28100
23	23500	0.046		
24	25600	0.007	24800	29100
	26800			
25	23600	0.022	22100	
	25700			
26	27000	0.026	29100	
27	23600	0.195	26600	28600
	24800			
	26000			
28			25300	27300
29			26100	27200

Results

Several different theoretical approaches were tested to evaluate if the optical spectrum of PICs could accurately be predicted. A number of different methods of geometrical optimization were used, AM1, PM3, and MM+. From X-ray crystallography¹ the symmetry was determined to be C_{2v} micro-symmetry in PICs **11-16c** and **16d** (Figure 3); this orientation occurs while the methyl groups are perpendicular to the plane of the ring system. PICs **1-10a** and **17-18c** have C_1 symmetry (Figure 3). Both AM1 and PM3 were unable to reproduce this C_{2v} micro-symmetry of PICs **11-16c** and **16d**. MM+ was able to more accurately reproduce this symmetry, which agrees with the X-ray crystallographic data. Proper geometric optimization is important since the symmetry will affect the electronic spectra. ZINDO/S was the only method available for the simulation of the electronic spectra.

The actual and theoretical excitation wavelength of PICs are listed in Table 3. The agreement between experimental and calculated excitation energies ranged from an error of 0.02 to 8.8 %, which is the similar to those obtained in a literature study of coumarins. The excitation maxima was taken to be the strongest oscillator wavelength line just before lowest triplet state. The actual excitation energies were determined in aqueous solution. Figure 5 is a fluorescent spectrum of PIC **2a**, whose optical properties are representation of the whole family of dyes.

The actual excitation maxima was measured in aqueous solution. The theoretical maxima was compared to the excitation maxima; this comparison is found in Figure 6. The theoretical excitation energies of PIC **14b** had the best agreement with the

experimentally determined values, (error 0.02 %). The poorest agreement obtained was with PIC **15b**, (error 8.8 %).

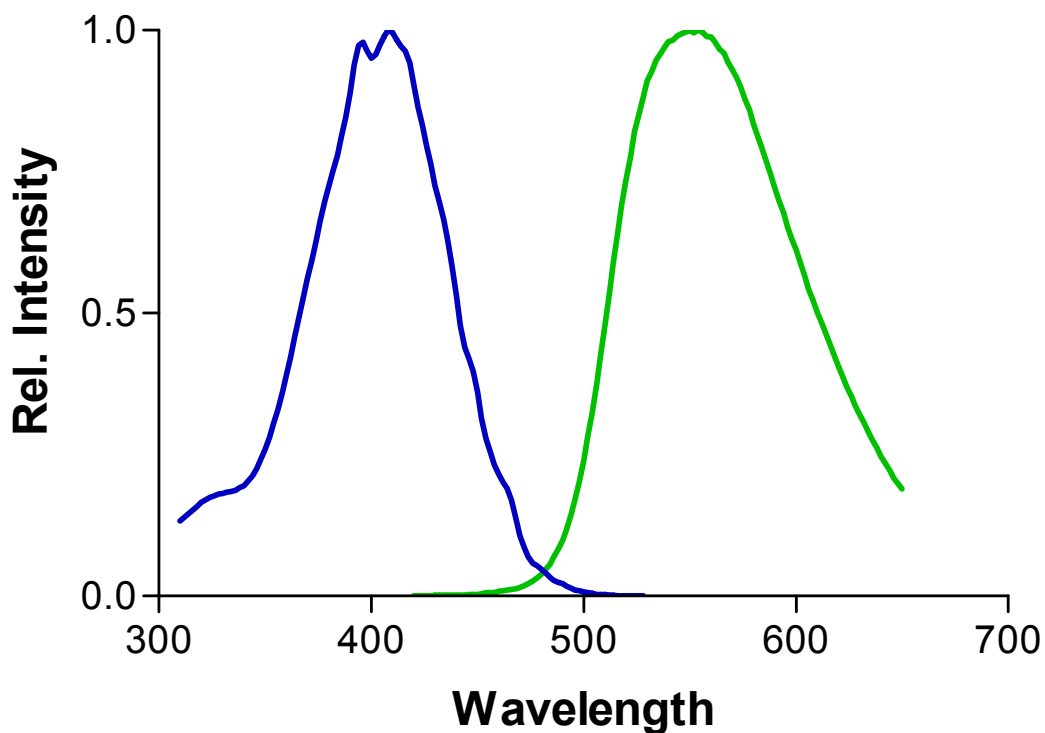


Figure 5: Excitation and emission maxima for PICs 1b

Table 3: Excitation maximum of each dye, their wavelength and strength and the actual excitation maximum

DYE NAME	Actual (nm)	Theory (nm)	Theory (cm ⁻¹)	Actual (cm ⁻¹)	Percent Error %
1a	433.7	425	23058.3	23529.4	2.0
2a	434.1	427	23036	21881.8	5.2
3a	436.6	425	22905.9	24449.9	6.3
5a	394.2	413	25367.9	25000	1.5
11b	434.1	425	23259.5	23529.1	1.1
12b	433.1	430	23087.2	23255.8	0.73
13b	443.4	445	22553.8	22471.9	0.36
14b	467.9	468	21371.4	21367.5	0.02
15b	419.17	447	22068.3	24213.07	8.8
17c	477.31	440	20951.7	22222.2	5.7
18c	477.29	440	20950.7	22222.2	5.7
19d	465.32	440	20951.7	22222.2	5.7

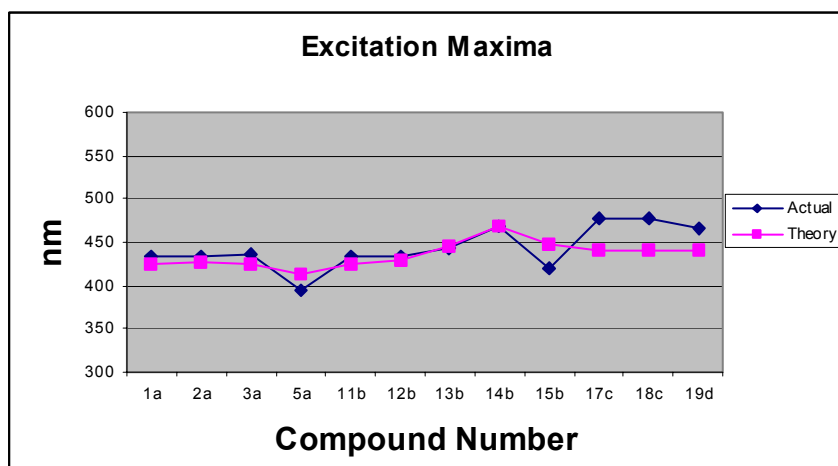


Figure 6: Actual excitation compared to theoretical excitation

The emission energies were computed using the same method as for the excitation energies. The results are summarized in Table 4. As with many organic dyes, the emission spectra of PICs are very broad (Figure 5), especially in aqueous solution. The emission maxima were difficult to simulate due to the large Stoke shift. The emission maxima were estimated to arise from photo emission from the first triplet state after the excitation. The agreement of theoretical emission and experimentally determination energies ranged from excellent to acceptable (error .18 to 7.8 %, Table 4). The experimentally determined emission energies vs. actual maxima are shown in Figure 7. The best agreement occurred with cation **5a** (error .10 %). PIC **3a**, showed the poorest correlation (error 7.3 %).

Dyes	Actual Emission (nm)	Theoretical Emission (nm)	Theoretical Emission (nm)	Actual Emission (nm)	Percent Error %
1a	494	519	19263.5	20242.9	4.8
2a	505	521	19230.4	19802	2.8
3a	490	529	18903	20408.2	7.3
5a	546	546	18315.1	20449.9	.18
6a	573.1		17449.9		
11b	533	552	18097.1	18761.7	3.5
12b	524	557	17950.7	19084	5.9
13b	571	571	17502.1	18148.8	.18
14b	626	625	15983.8	14814.8	.18
15b	540	540	18512.5	18181.8	.18
17c	550	562	17776.6	22222.2	2.1
18c	550	557	17943.9	22222.2	2.1
19d	550	566	17666.7	22222.2	2.1

Table 4: Theoretical and actual emission maximum

Almost all theoretical emission maxima were at lower energy than actual emission maxima. This was not the case in the study of coumarins. This was likely caused by the way the emission maxima were determined, which was the first triplet state after the excitation maxima. This methodology of using the triplet was used since the computational methodology was unable to correctly evaluate the PICs system because of its unusually large Stoke shift (100 nm). Due to this problem there were no singlets, only triplets, where the expected emission maxima should have been located. So it was theorized that this triplet state did in fact exist in the molecule. The 77 K spectrum of PIC **2a** (Figure 4) shows a shoulder on the emission maxima, which is thought to be a triplet state. The triplet is lower in energy than the expected singlet; this insures that the prediction of emission maxima is at a longer wavelength than the actual maxima in normal fluorescent. The only exception is dye **14b**; this is the only red dye (675 nm) in the family of dyes. Dye **14b**'s stoke's shift is unusually large even for this family of dyes

(200 nm), this astronomically large shift may break down the computational methodology.

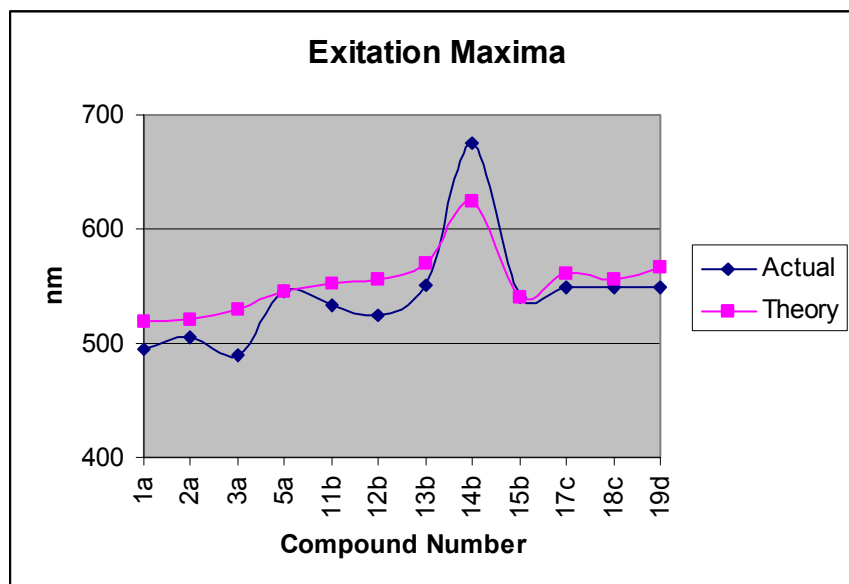


Figure 7: Actual emission maximum compared to actual emission maximum

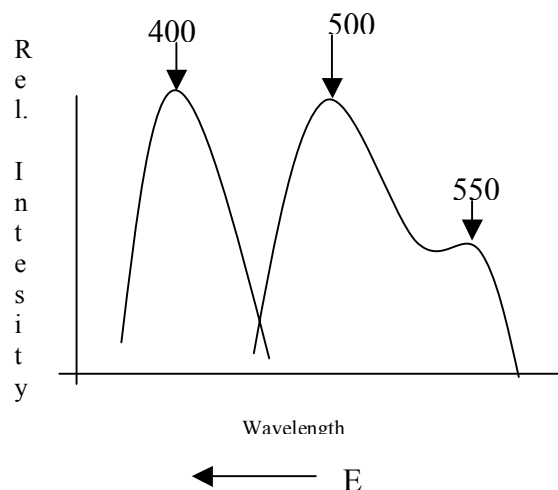


Figure 8: A representation of the shoulder on the 77 K data.

Methods

Chemical structures were drawn with Isis Draw software.¹² The structure was imported into HyperChem 6.0. A log was then initiated for the purpose of recording the results and a sample is contained in Appendix I. Optimization was performed, using MM+. Once an optimization for PICs **11-16b** and **19d** agreed with the known symmetry (C_{2v}), an electronic spectra was obtained. PICs **1-10a** and **16-17c** were optimized to give known symmetry (C_1), then an electronic spectra was obtained. The parameters for semi-empirical methods were set according to Table 5.

	PICs 1-16	PICs 17-18
Total Charge	1	2
Multiplicity	1	1
Spin Pairing	RHF	RHF
State	Lowest	Lowest
Weight factor $\sigma-\sigma$	1.267	1.267
Weight factor $\pi-\pi$	0.585	0.585
Occupied Orbitals	5	5
Unoccupied Orbitals	5	5

Table 5: Parameter for semi-empirical methods

The electronic spectra was calculated with the use of the semi-empirical method Zindo/s. The excitation wavelength was determined to be the strongest oscillator line in the spectra just before the lowest triplet state. The emission maxima was determined to arise from photo emission from the first triplet state after the excitation.

This work has been used to identify a potential red fluorescent dye, **6a**; low molecular weight red fluorescent dyes would potentially be useful in imaging cells. The

theoretical data shows that amino groups in the 4 and 4' position of the pyridine ring would result in the longest wavelength emission.

Conclusion

The actual excitation maxima were measured in the aqueous solution. The theoretical maxima and the excitation maxima were compared in Figure 6. The theoretical excitation energies of PIC **14b** had the best agreement with the experimentally determined values, (error 0.02 %). The poorest agreement obtained was with PIC **15b** (error 8.8 %).

The agreement of theoretical emission energies and experimentally determined values obtained ranged from excellent to acceptable (error .18 to 7.8 %, Table 4). The experimentally determined emission energies were compared to the actual emission energies, as shown in Figure 7. The best agreement occurred with compounds **5a** (error .10 %). PIC **3a** showed the poorest correlation (error 7.3 %).

Computational methods were effective in the prediction of both absorption and emission maxima in the PICs system with reasonable accuracy. These computational calculations provide a valuable tool in the rational design of optical properties of dyes in our laboratories with the goal of longer wavelength dyes.

Chapter 2: Synthesis of fluorescent dyes

Introduction

The majority of PICs (Figure 3) prepared in our laboratory are violet excitable green fluorescent dyes (490-540 nm). For many applications, including intracellular studies, longer wavelength dyes (<600 nm) are advantageous. Amino derivatives of fluorescent compounds generally have shown a red shifted fluorescence compared to the parent fluorophore. This lowering of the emission energy is due to the influence of the lone pair of electrons on the amino nitrogen atom on the energy of the entire ring system. The effect of aminating green fluorescent PICs will be explored. PICs 1 were chosen because there seemed to be multiple ways in which amination can be accomplished, and in multiple positions, using straightforward synthetic methodology. An additional motivation for preparing amino substituted PICs is that it offers several routes to the preparation of an isothiocyanate.

A survey of the literature revealed that Newkome¹³ and co-workers developed a methodology toward the preparation of a 5-amino-substituted 2-2'bipyridine (Figure 9). The methodology could be applied to the pyridylquinoline ester, **2a**, (Figure 10) giving the amino pyridyl-quinoline ester, **8a**, **10a**, (Figure 11). A survey of the literature revealed that Hawthorne¹⁴ and co-workers reported a method of making an amine into an isothiocyanate.

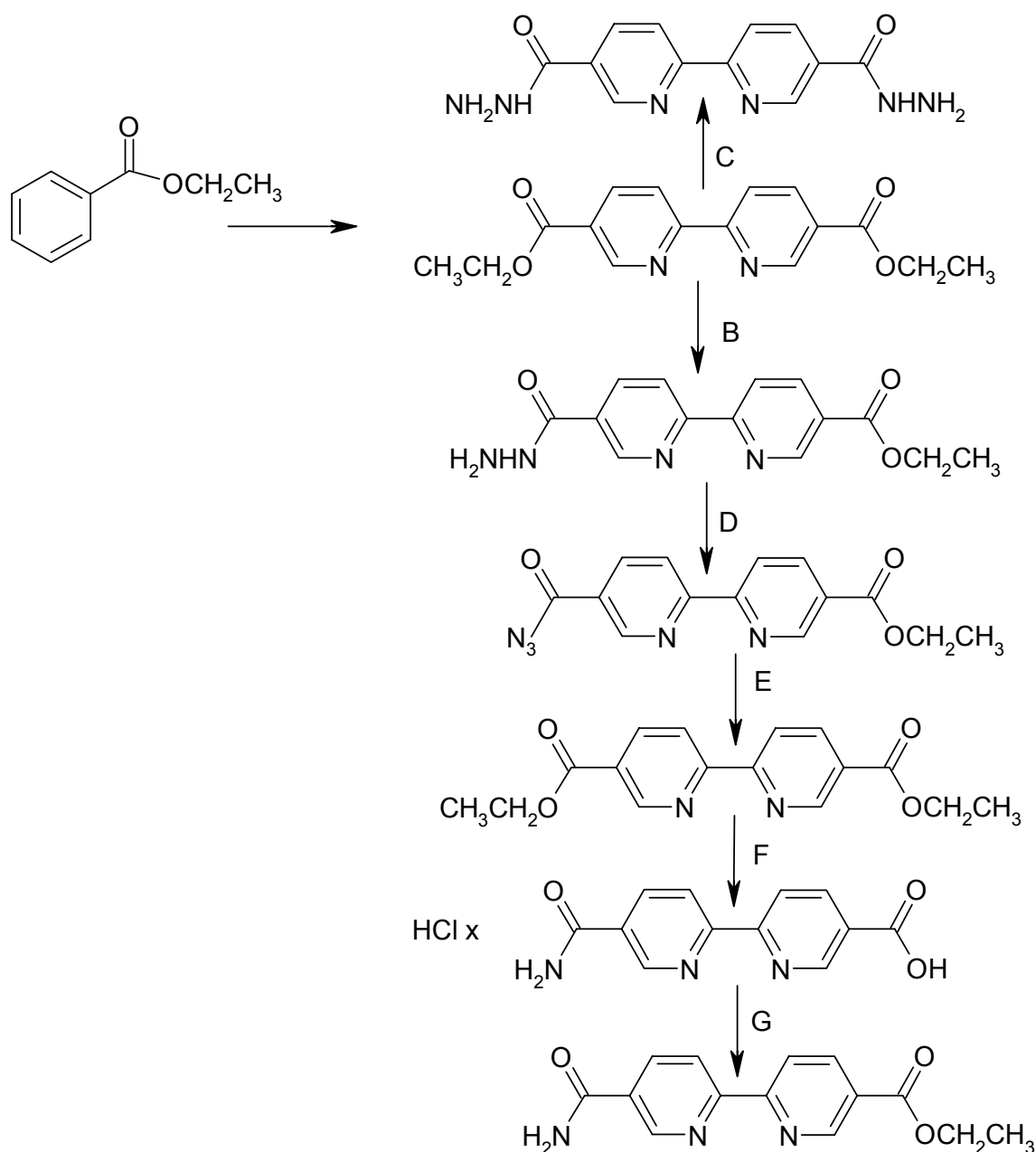


Figure 9: Scheme 1 (a) 10% Pd/C (b) 1.5 equiv of NH_2NH_2 , EtOH, toluene, 115°C (d) HCl, 0°C , aqueous NaNO_2 (e) EtOH, xylene, reflux (f) EtOH, 2.5 M NaOH, 75°C (g) con. H_2SO_4

The ester functionality was synthetically manipulated into an amine in multiple high yield steps (Figure 10), with the key step being a Curtius rearrangement of the azide, **3a**, into the ethyl carbamate, **4a**. This methodology was chosen based on the work of

Newkome¹⁴ in a similar synthesis of a 5-aminosubstituted bipyridine (Figure 9). Newkome showed that a Curtius rearrangement in these related compounds could be extremely effective. Thus, in our preparation of a 4-amino-2-(2-pyridyl)-4-aminoquinoline, **5a**, this methodology was an obvious starting point. In practice the strategy worked extremely well. All of the steps went in good to very good yield, could easily be adopted to large scales, required no chromatographic separations, and produced the target amine in an overall yield of (35%) from 4-carboxymethyl-2-(2-pyridyl)-quinoline.

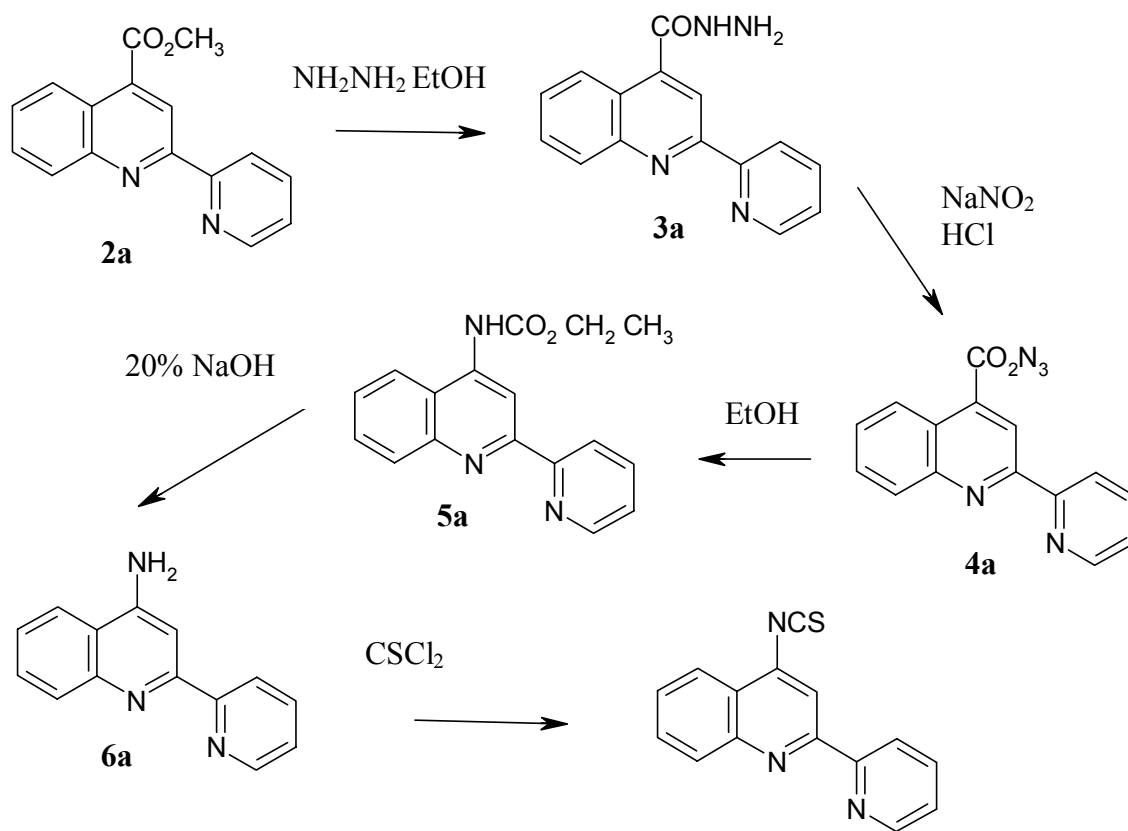


Figure 10: Scheme used to synthesize amino PICs

The second approach toward an amino substituted pyridyl-quinoline derivative was to directly nitrate the ester, **2a**, followed by reduction of the nitro group (Figure 11). Nitration of the ester, **2a**, gave a set of isomers in a 1:1 mixture, that were unable to be separated. Reaction temperature had little or no effect on the ratio of isomers. It was reasoned that the amines might be easier to separate than the corresponding nitro compounds. The nitro mixture was reduced with PtO_2 to the amino compounds. This approach proved to be successful on 4-carboxymethyl-8-amino-2-(2-pyridyl)quinoline, **10a**, because it was soluble in methylene chloride. All of the steps in Figure 11 went in good yield, required no chromatographic separations, and produced the target amine in an overall yield of (41%).

Part of this research was targeted the preparation of a fluorescent isothiocyanate PIC dye. In 1941 Albert Coons developed the fluorescent isothiocyanate immunofluorescence technique.¹⁵ Immunofluorescence involves the attachment of a fluorescent dye to an antibody with the use of an isothiocyanate group. Isothiocyanates are known to be chemically reactive with nucleophilic groups on proteins. The isothiocyanate was to be prepared from the amino compound, **5a**. The methodology proposed by Hawthorne¹⁴ was attempted, which utilized thiophosgene. The attempt was unsuccessful in yielding the expected isothiocyanate. The reaction was attempted under nitrogen and in air; neither was effective. Also, other reaction conditions were tried using thiophosgene and were also ineffective.

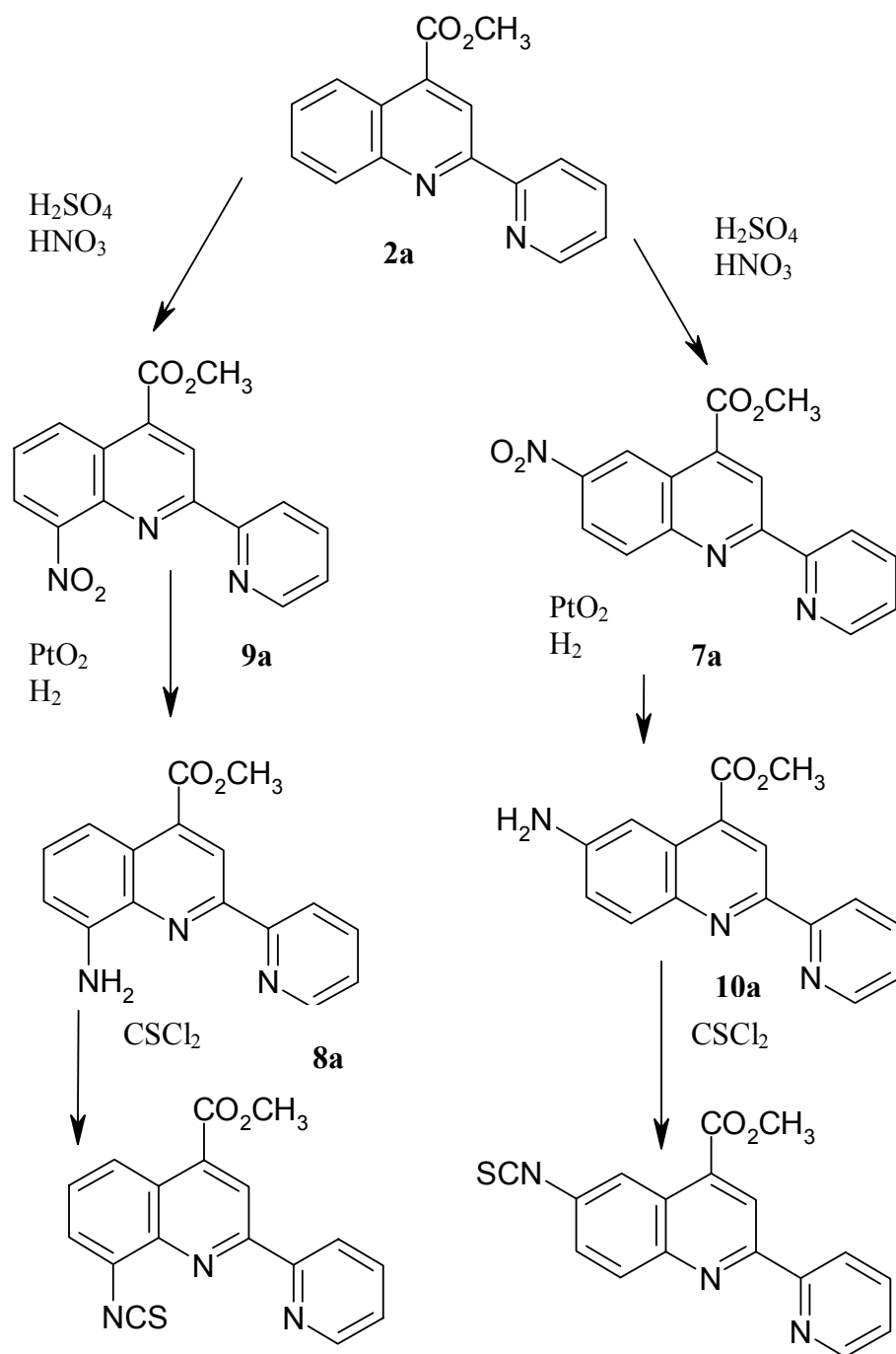


Figure 11: Synthesis of Amino-ester PICs

Experimental

All chemicals were purchased from chemical suppliers and used without further purification, unless noted

4-Carbohydrazido-2-(2-pyridyl)quinoline, **3a**

To a 1 L round bottomed flask was added 10.1g of 4-carboxymethyl-2-(2-pyridyl)-quinoline, **2a** (19.0 mmol) 50 mL of xylene, 30 mL of ethanol, and 30 mL of hydrazine hydrate was added. The stirred solution was refluxed for 20 hours. The flask was cooled to 5 °C and the solid filtered, and allowed to air dry, giving 6.5 g of **3a** as a bright white solid (65%) mp. 221-223 °C. ¹H NMR (DMSO-d₆) (Figure 12) COSY (Figure 13) δ = 10.0 (s, 1 H, NH); 8.78 (d, 1 H, J = 4.5, H-d); 8.63 (d, 1 H, J = 7.5, H-a); 8.56 (s, 1 H, H-o); 8.18 (d, 1 H, J = 8.5, H-4); 8.21 (d, 1 H, J = 8.5, H-1); 8.04 (ddd, 1 H, J = 2,1.5,8,8, H-b); 7.86 (ddd, 1 H, J = 1,2,1.5,7,8,7.5, H-3); 7.70 (ddd, 1H, J = 1,2,1.5,7,8,7.5, H-2); 7.56 (ddd, 1 H, J = 1.5,1.5,7.5, H-c) 4.75 (s, 2 H, NH₂) ¹³C NMR (DMSO-d₆) δ = 165.99, 154.98, 154.57, 149.37, 147.54, 142.08, 137.51, 130.27, 129.61, 127.65, 125.46, 124.93, 124.50, 121.07, 116.47 IR NH₂ (3425 cm⁻¹)

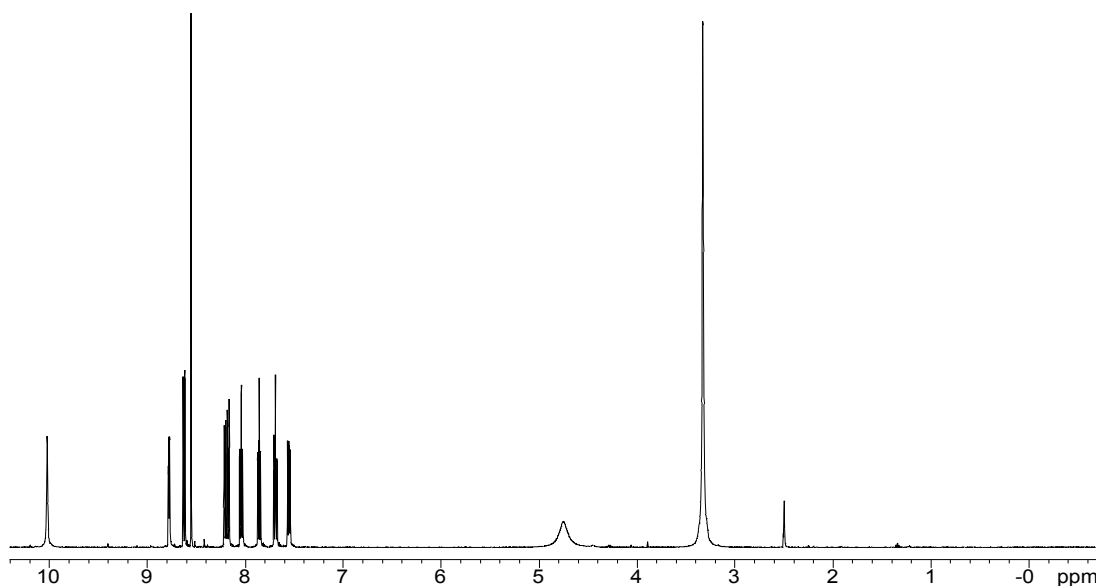


Figure 12: ¹H 500 MHz NMR of 4-carbohydrazido-2-(2-pyridyl)quinoline.

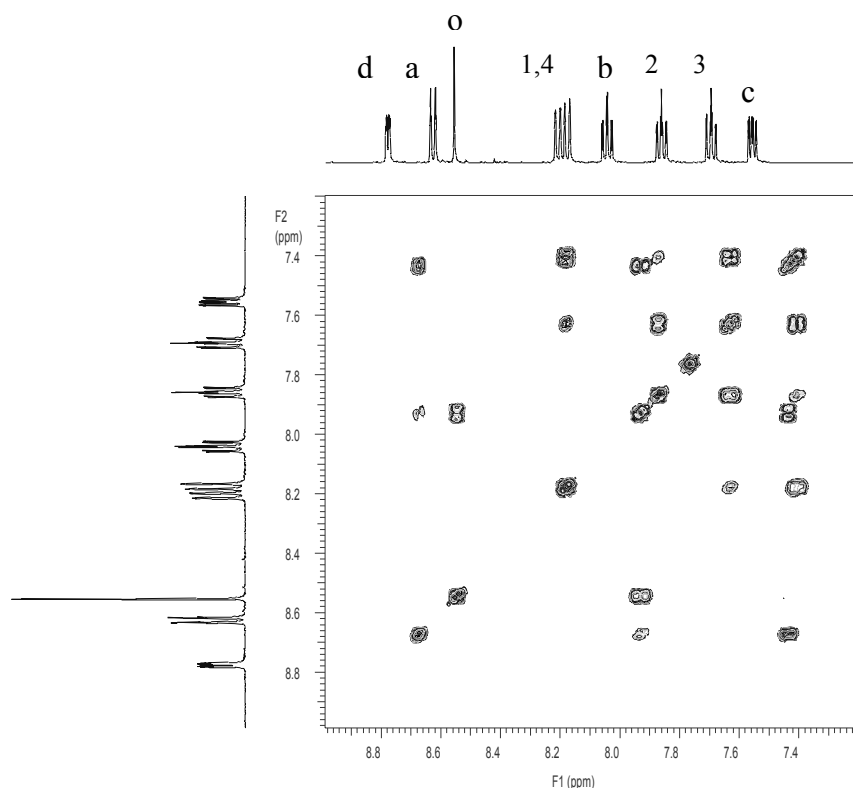


Figure 13: ^1H COSY 500 MHz NMR of 4-carbohydrazido-2-(2-pyridyl)quinoline

4-Carbazido-2-(2-pyridyl)quinoline, **4a**

A two neck 1 L round bottomed flask was fitted with a magnetic stirrer, a thermometer, and a pressure equalized dropping funnel. The flask was charged with 90 mL of con HCl and 6.4 g (10 mmol) of 4-carbohydrazido-2-(2-pyridyl)quinoline, **3a**. The solution was cooled to 0 °C in an ice bath. The funnel was charged with a solution of 30 g (432 mmol) of sodium nitrite in 200 mL of water. With stirring, the solution of sodium nitrite was added to the flask at a rate such that the temperature remained below 5 °C. Too high a rate of addition causes foaming to occur, particularly if the temperature rises too swiftly. During the addition the color of the solution changes from a bright yellow to a burnt orange. Following the addition of the sodium nitrite solution, stirring was continued for an additional 15 minutes at 0 °C, and 1 hour at room temperature. At this

point there the solution had a pale yellow coloration with a thick white precipitate. The addition funnel was charged with a solution of 10% NaOH, and 100 g of ice was added to the flask. The reaction mixture made basic. Small portions of ice were added to the flask so as to maintain the temperature below 2 °C throughout the neutralization. The pale white precipitate **3a** was collected by suction filtration, washed liberally with water (3 X 100 mL, placed in a 100 mL round bottomed flask and dried under vacuum at 20 °C. giving **4a** as a white solid, which was found to be thermally stable up to 95 °C (5.5 g, approximately 68%). It was purified, but used immediately in the preparation of **5a**.

4-Ethylcarbamato-2-(2-pyridyl)quinoline, **5a**

To a 100 mL round bottomed flask, was added 4-carbazido-(2-pyridyl)quinoline, **4a**, 40 mL of xylene and 30 mL of absolute ethanol. The mixture was refluxed for 6 hours. The temperature was closely controlled to avoid severe frothing when the reaction mixture was refluxing. The mixture was then cooled to room temperature, and the volume reduced on a rotory evaporator until a thick white precipitate appeared. At this point the mixture was cooled to 5 °C and filtered, giving the carbamate ester, **5a**, as a white solid mp 171-173 (65 % yield). ¹H NMR (DMSO-d₆) (Figure 14) COSY (Figure 15) δ = 8.78 (d, 1 H, J = 4.5, H-d); 8.62 (d, 1 H, J = 8, H-a); 8.55 (s, 1 H, H-o); 8.21 (d, 1 H, J = 8, H-4); 8.18 (d, 1 H, J = 8.5, H-1); 8.04 (ddd, 1 H, J = 1.5,2,8,8, H-b); 7.86 (ddd, 1 H, J = 1.5,2.5,1,7.5,8, H-3); 7.70 (ddd, 1 H, J = 1.5,2.5,1,7.5,8,7.5, H-c); 7.55 (ddd, 1 H, J= 1,1.5,5,5,7.5) 4.34 (t, J = 5, CH₃) 3.42 (q, J = CH₂) δ =165.99, 154.98, 154.56, 149.36, 147.54, 142.08, 137.49, 130.25, 129.60, 127.64, 125.45, 124.92, 124.49,

121.06, 116.46, 55.98, 18.49 IR NH (3462 cm^{-1})

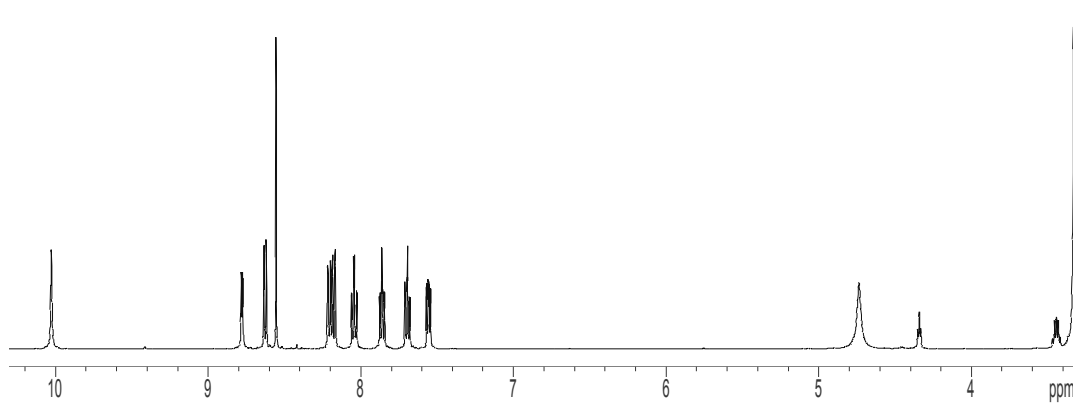


Figure 14: ^1H 500 MHz NMR of 4-ethylcarbamato-2-(2-pyridyl)quinoline.

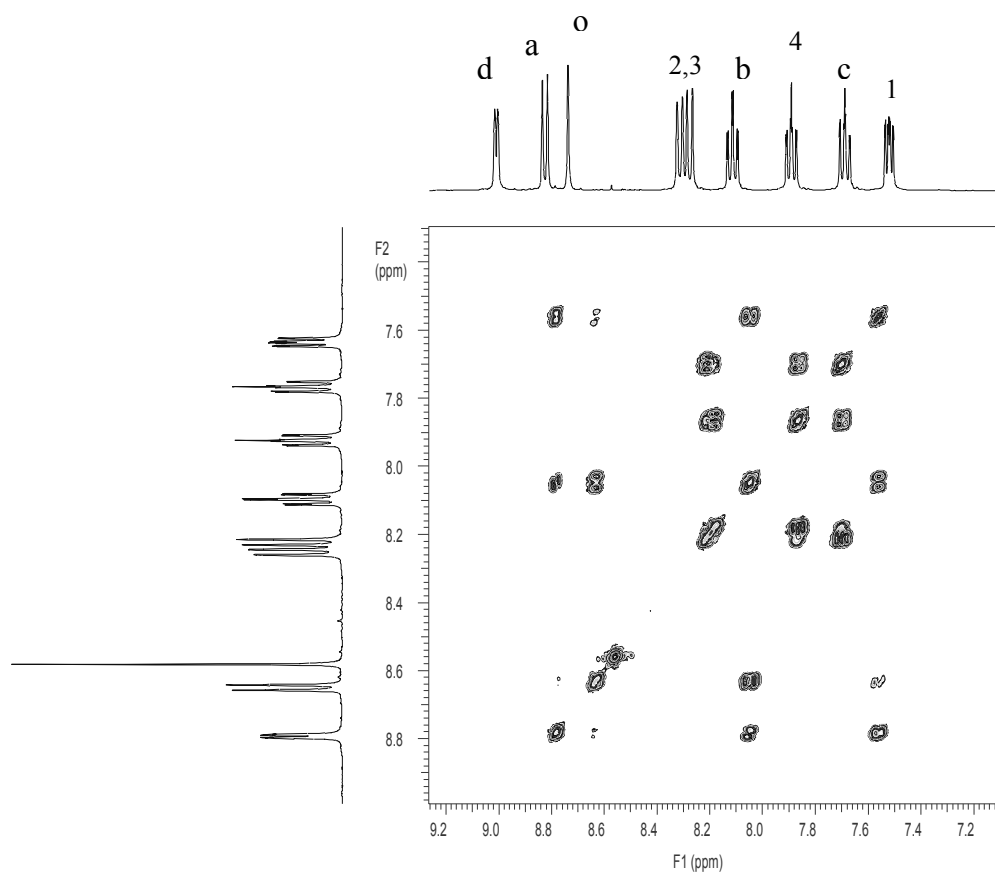


Figure 15: ^1H - ^1H COSY 500 MHz NMR of 4-ethylcarbamato-2-(2-pyridyl)quinoline

4-Amino-2-(2-pyridyl)quinoline, **6a**

A stirred solution of 4-ethylcarbamate-2-(2-pyridyl)-quinoline, **5a**, (5.0 g) in a mixture of ethanol (50 mL) and 2.5 N aqueous NaOH (50 mL) was heated at 75°C for 14 hours. The ethanol was concentrated in a rotary evaporator, and the result white precipitate, **6a**, (67%) was vacuum filtered, washed with cold water, and air-dried. ^1H NMR (DMSO- d_6) (Figure 16) COSY (Figure 17) δ = 8.68 (d, 1 H, J = 5, H-d); 8.54 (d, 1 H, J = 8, H-a); 8.18 (d, 1 H, J = 8.5, H-4); 7.67 (dd, 1 H, J = 8, 7.5, H-2); 7.93 (ddd, 1 H, J = 1.5, 7.5, 8, 7.5, H-b); 7.87 (d, 1 H, J = 8.5, H-1); 7.77 (s, 1 H, H-0); 7.4 (m, 1 H); 7.4 (m, 1 H) 6.9 (s, 2 H, NH_2) δ = 156.26, 155.35, 148.82, 148.53, 136.81, 129.26, 129.19, 123.92, 123.85, 122.25, 120.79, 118.53, 99.21, 30.61. IR NH_2 (3375 cm^{-1})

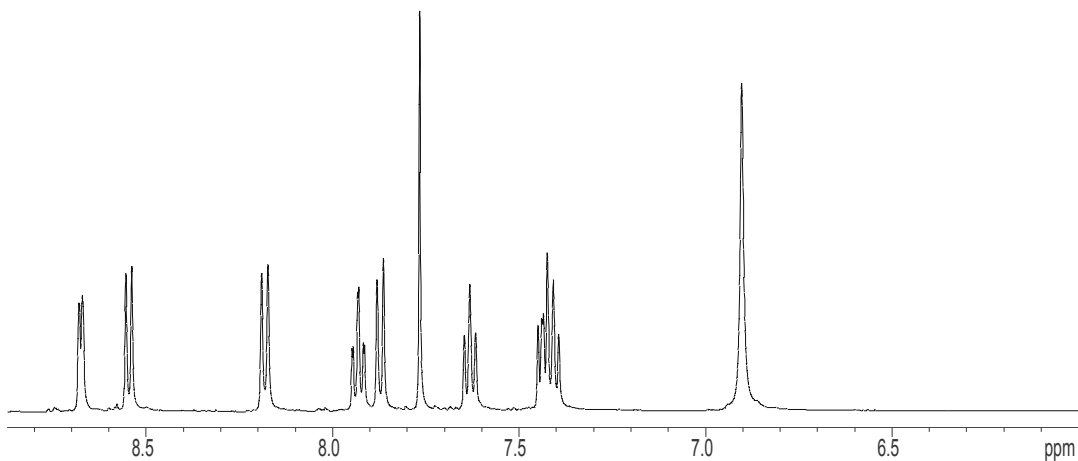


Figure 16: ^1H 500 MHz NMR of 4-amino-2-(2-pyridyl)quinoline

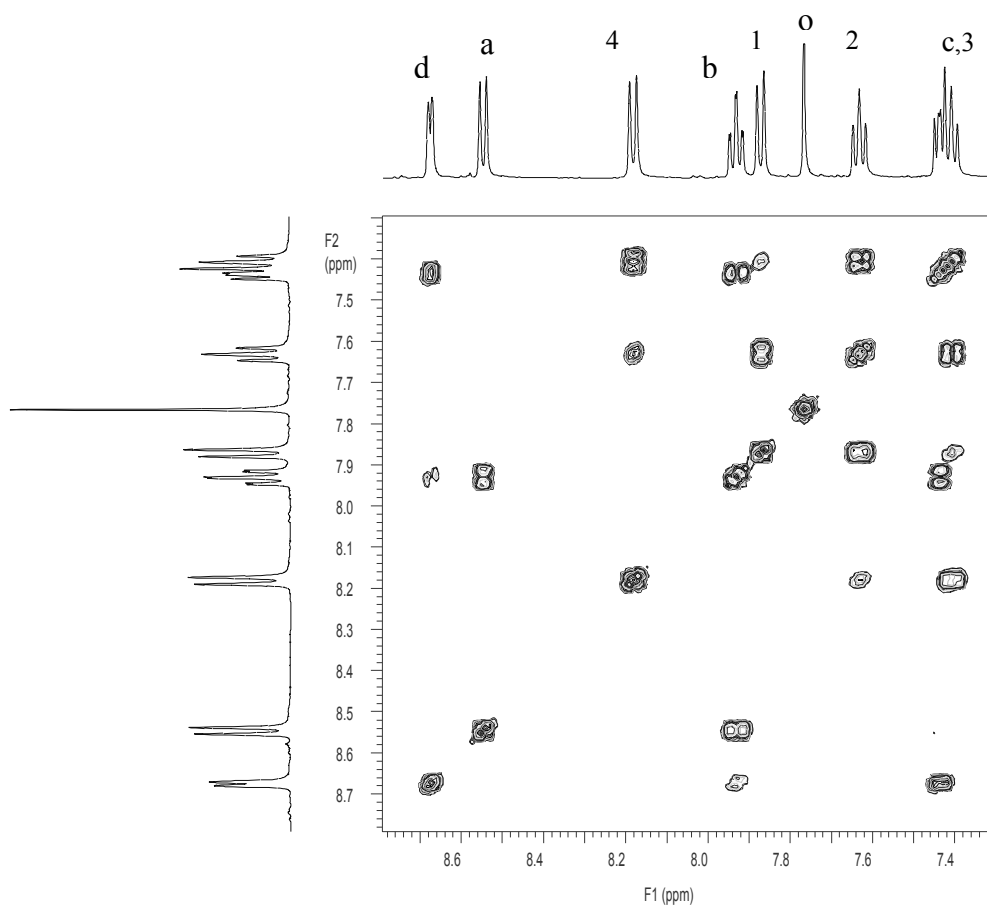


Figure 17: ^1H - ^1H COSY 500 MHz NMR 4-amino-2-(2-pyridyl)quinoline

Mixture of 4-Carboxymethyl-6-nitro-2-(2-pyridyl)quinoline, **7a**, and 4-Carboxymethyl-8-nitro-2-(2-pyridyl)quinoline, **9a**

A two neck 250 mL round bottomed flask was fitted with a magnetic stirrer a thermometer, and a pressure equalized dropping funnel, to the flask was added 25 mL of con sulfuric acid and 5.0 g (4.0 mmol), of 4-carboxymethyl-2-(2-pyridyl)quinoline, **2a**. The solution was cooled to 0 $^{\circ}\text{C}$ in an ice bath. The addition funnel was charged with a solution of 25 mL of con nitric add. With stirring, the nitric acid was added to the flask at a rate such that the temperature remained below 5 $^{\circ}\text{C}$. Following the addition, stirring was continued for an additional 15 minutes at 0 $^{\circ}\text{C}$, and 30 minutes at 50 $^{\circ}\text{C}$. This mixture

poured over 100 g of ice and neutralized with 10% NaOH. The precipitate was collected by filtration washed liberally with water and allowed to dry, giving the nitro compounds, **7a**, **9a**, as a pale yellow solid (5.2 g, 86%), which was found to be a mixture of isomers. The isomers were 4-Carboxymethyl-6-nitro-2-(2-pyridyl)quinoline, **7a** and 4-Carboxymethyl-8-nitro-2-(2-pyridyl)quinoline, **9a**, (Figure 18). The COSY spectra are in Figure 19. 4-Carboxymethyl-8-nitro-2-(2-pyridyl)quinoline, **7a**, $\delta = 9.062$ (s, 1 H, J = 5, H-o), 9.046 (d, 1 H, J = 1, H-9), 8.743 (ddd, 1 H, J = .5, 1, .5, 1.75, 5, H-k), 8.638 (dd, 1 H, J = 1, 1.5, 1.25, H-i), 8.050 (dd, 1 H, J = 1, 7.5, H-11), 7.883 (m, 1 H), 7.696 (dd, 1 H, J = 7.5, 9), 7.409 (m, 1 H) IR NO₂ (1529, 1381 cm⁻¹) 4-Carboxymethyl-8-nitro-2-(2-pyridyl)quinoline, **9a**, ¹H NMR $\delta = 9.250$ (s, 1 H, H-o), 8.771 (ddd, 1 H, J = .5, 1, .75, 1.5, 5, H-d), 8.653 (dd, 1 H, J = 1, 1.5, 1.25, H-b), 8.540 (dd, 1 H, J = 1.5, 8.5, H-3), 8.172 (dd, 1 H, J = 1.5, 1, 7.75, H-1), 7.904 (m, 1 H), 7.815 (dd, 1 H, J = 7.5, 8.5, H-2), 7.424 (m, 1 H)

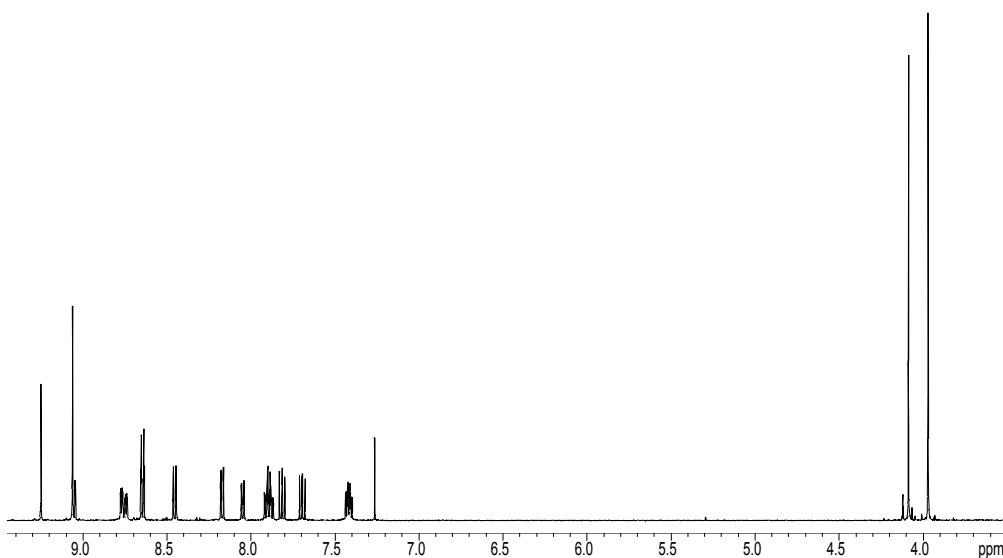


Figure 18: ¹H 500 MHz NMR of 4-carboxymethyl-8-nitro-2-(2-pyridyl)quinoline and 4-carboxymethyl-6-nitro-2-(2-pyridyl)quinoline

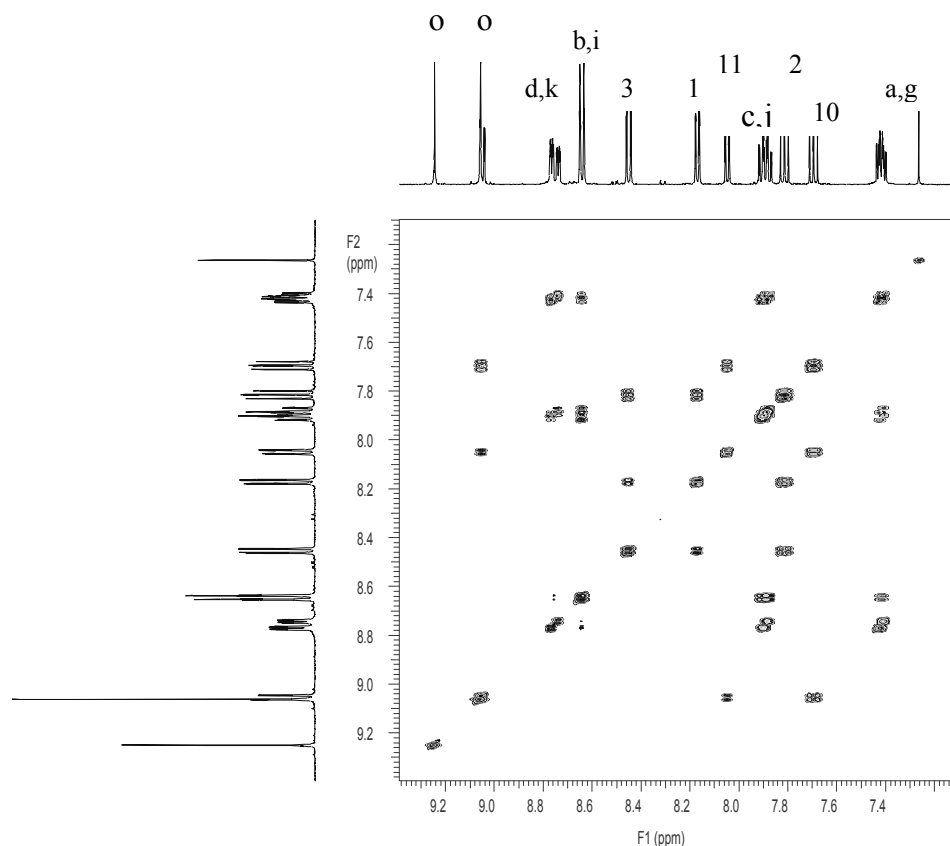


Figure 19: ^1H COSY 500 MHz NMR of 4-carboxymethyl-8-nitro-2-(2-pyridyl)quinoline and 4-carboxymethyl-6-nitro-2-(2-pyridyl)quinoline

Mixture of 4-Carboxymethyl-6-amino-2-(2-pyridyl)quinoline, **8a**, and 4-Carboxymethyl-8-amino-2-(2-pyridyl)quinoline, **10a**,

In a Parr bomb, 5.0 g (4.0 mmol) of 4-Carboxymethyl-8-nitro-2-(2-pyridyl)quinoline, **7a**, and 4-Carboxymethyl-6-nitro-2-(2-pyridyl)quinoline, **9a**, and 0.40 g of platinum oxide were added into methanol. Hydrogen gas was added at a pressure of 2 atm. The reaction was stirred for 2 hours at room temperature. The solution was filtered and the methanol was evaporated. The compound 4-carboxymethyl-8-amino-2-(2-pyridyl)-quinoline, **10a**, was soluble in methylene chloride. Compound 4-carboxymethyl-6-amino-2-(2-pyridyl)-quinoline, **8a**, was soluble in DMSO. IR NH_2 (3395 cm^{-1}) 4-Carboxymethyl-amino-2-2-pyridyl-quinoline, **8a**, (Figure 20) COSY (Figure 21) $\delta = 9.02$ (s, 1 H, H-o), 8.59 (ddd, 1H, H-d), 8.740 (m, 1 H, H-a) 8.038 (dd, 1

H, H-3), 7.846 (ddd, 1 H, H-c), 7.432 (dd, 1 H, H-2), 7.350 (ddd, 1 H, H-b). 6.978 (dd, 1 H, H-1), 5.25 (s, 2 H, NH₂) ¹³C) δ = 155.934, 149.504, 137.250, 130.613, 130.042, 128.353, 125.781, 52.827 125.325, 124.580, 121.922, 120.536

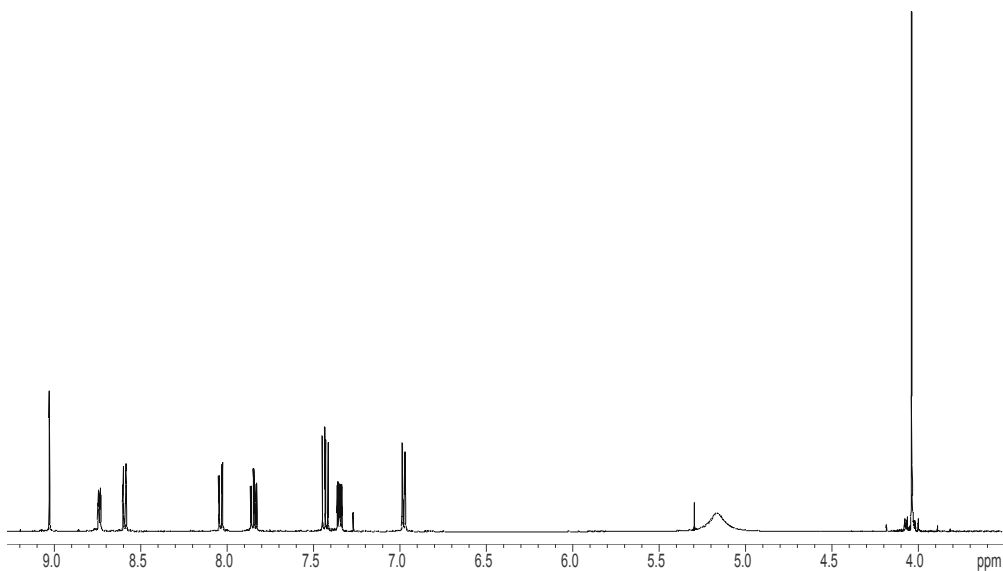


Figure 20: ¹H 500 MHz NMR of 4-carboxymethyl-8-amino-2-(2-pyridyl)quinoline

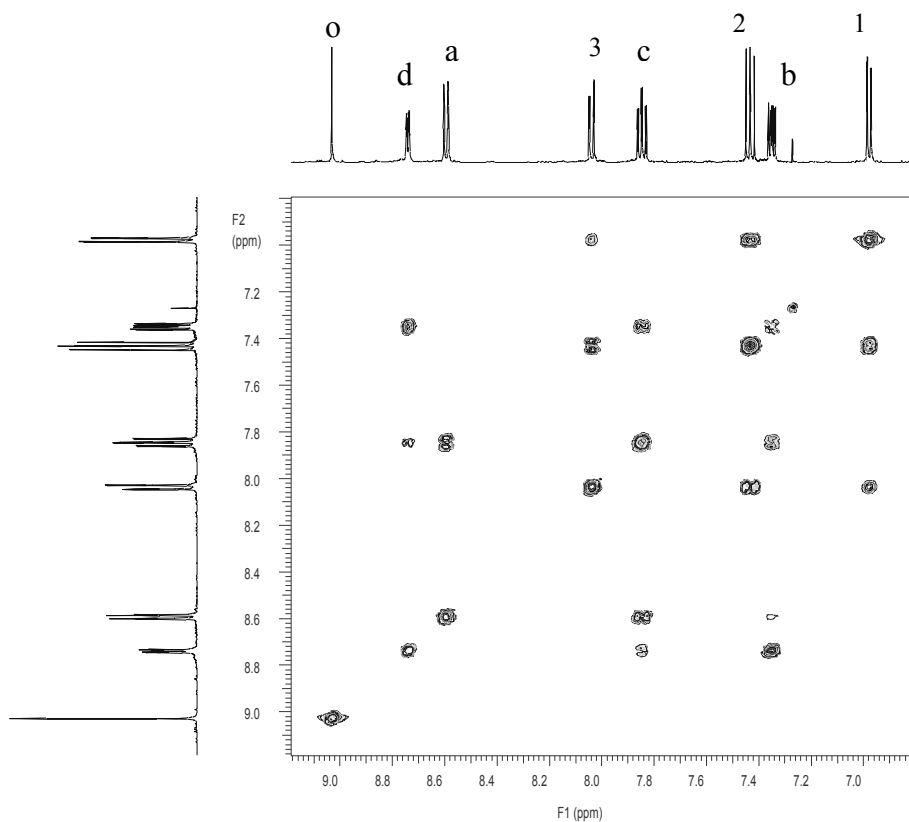


Figure 21: ¹H-¹H COSY 500 MHz NMR of 4-carboxymethyl-8-amino-2-(2-pyridyl)quinoline

Results and Discussion

The methodology developed by Newkome¹⁴ (Figure 9) proved to be effective on our system (Figure 10). All steps in the preparation of **5a** (Figure 9) gave a satisfactory yield (approximately 70%) and good purity. The compound 4-amino-2-(2-pyridyl)quinoline, **5a**, was characterized by assigning all of the hydrogens (Figure 22) with the use of COSY NMR and the splitting patterns. COSY NMR is a two dimensional technique which monitors the hydrogen-hydrogen interactions. Hydrogens on the pyridine rings were assigned letters and the hydrogens on the quinoline ring were assigned numbers (Figure 22). COSY NMR allows for the determination of what hydrogens are side by side and the placement of weakly coupled hydrogens. Chemical shift knowledge is also needed in the assignment of hydrogens. In **5a** (Figure 17), the hydrogen most down field is hydrogen d, which would strongly interact with hydrogen c and weakly interact with hydrogen b. A COSY NMR spectra is interpreted the following way, if hydrogen d is followed straight down and hydrogen c is noted by a large dot (strong coupling) and hydrogen b is noted by a relatively small dot (weak coupling). Also in the spectrum there is a dot where hydrogen d interacts with itself. All the hydrogens interacting with themselves forms a diagonal line in all COSY spectrum from the bottom left corner and goes to the top right corner. Once all the hydrogens associated with the pyridine ring had been assigned this left only the hydrogens associated with the quinoline ring. The hydrogens associated with the quinoline ring were assigned the same manner as the pyridine ring. This is the way the hydrogens in all compounds were assigned. FT-IR was used to confirm the presence of an amine group 3375cm^{-1} .

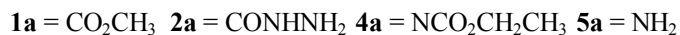
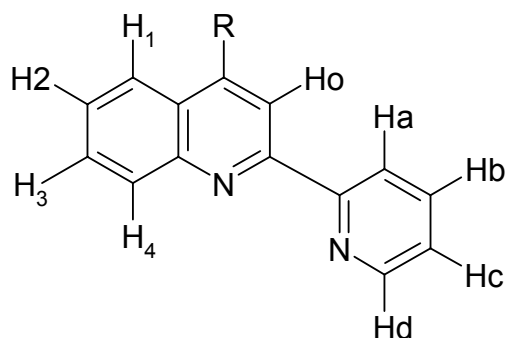
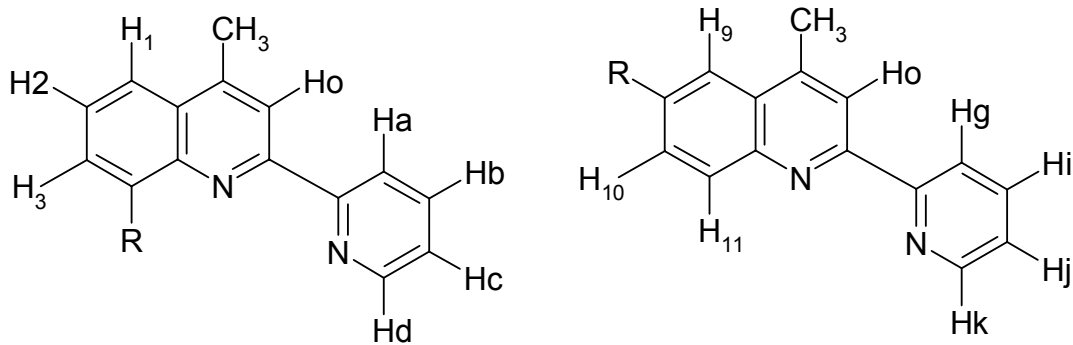


Figure 22: Base structures for assignment by 1H COSY

The combination of ¹³C, ¹H, and COSY NMR were used to confirm the nitration of 4-carboxymethyl-2-(2-pyridyl)quinoline yielded a set of isomers. The isomers were 4-carboxymethyl-8-nitro-2-(2-pyridyl)quinoline, **9a**, and 4-carboxymethyl-6-nitro-2-(2-pyridyl)quinoline, **7a**. Using COSY and splitting patterns all hydrogens were assigned on the pyridyl-quinoline in the same manner as **5a** (Figure 23). The reduction of the amine with hydrogen yielded the expected isomeric amines. The 4-carboxymethyl-8-amino-2-(2-pyridyl)quinoline, **10a**, was soluble in dichloromethane therefore it was possible to separate the isomers. The 4-carboxymethyl-6-amino-2-(2-pyridyl)quinoline, **8a**, was not been purified, due to the poor solubility. The nitro compounds were non-fluorescent. Both amino compounds were fluorescent. As expected, the amino group in both cases did affect the fluorescence spectra causing a red shift of 50 nm.



7 = NO₂
8 = NH₂

Figure 23: Base Structures of the assignment of the isomer mixtures

Conclusion

The presences of amino groups on a known fluorescent ring system are well established to markedly affect the optical properties of the dye. Methodology has been developed for the amination of different position on the 2-(2-pyridyl)-carboxyquinoline ring system(4-Carboxymethyl-6-amino-2-(2-pyridyl)quinoline, **8a**, and 4-Carboxymethyl-8-amino-2-(2-pyridyl)quinoline) **11a**, leading to the testing of three new amino substituted fluorescent dyes. Another methodology was effect in the synthesis of 4-amino-2-(2-pyridyl)quinoline, **6a**. This is also the precursor to 4-isothiocyanato-amino-2-(2-pyridyl)quinoline, which can be used as a cellular tag for proteins.

Chapter 3: Confocal Imaging

Introduction

Conventional microscopes are capable of creating images with a depth of field of 2-3 μm . Due to the limited resolving power of most optical microscopes, it is possible to have several objects in the same depth of field producing superimposition of those objects. Superimposition causes a loss of structural details. Superposition of objects causes halos to form around objects of interest. This is especially prominent in fluorescent microscopes. In contrast, confocal microscopes create optical sections, which are 0.5 μm or less thick. This allows for rejection of light out of the focal plane, which minimizes the obscuring of image details¹⁶ (Figure 24). Confocal microscopes have become an increasingly essential analytical tool for the study of the structure and physiology of living cells.

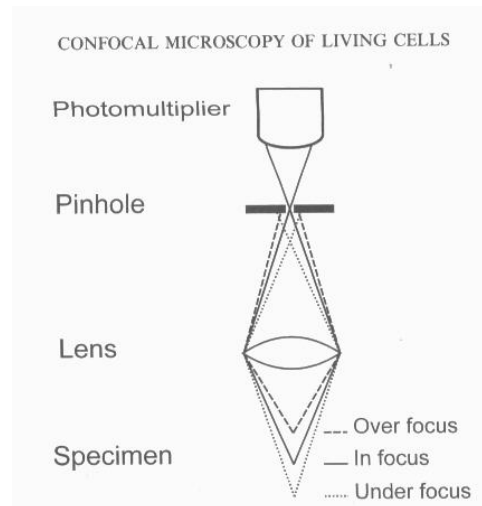


Figure 24: How a Confocal Microscope works

The use of small fluorescent molecules as molecular probes has gained acceptance as one of the most important general methods of obtaining information on cellular structure and function. The pattern of their fluorescence throughout the cell is captured as an image representing a 0.5 μm thick slice of the cell. The combination of many such slices results in a three dimensional image of the cell.

A problem with fluorescent probes is to have the right dye localize in the portion of the cell that is of interest to the observer. Other problems associated with confocal microscopy are photo bleaching and degradation of cells. Photo bleaching is the irreversible destruction of a fluorophore, which decreases the intensity of the dye inside the cell. All dyes have different rates of photo bleaching. With live cells the laser power is very likely to damage and/or kill the cell. Even with all these problems there are hundreds of fluorescent dyes listed in catalogues. Dyes are listed according to their application area (ion-sensitive, membrane potential, etc.) and the organelle in which the dye localize, also included with each dye is a list of literature references.¹⁷ Dyes are subdivided into dyes that stain live cells and those that stain fixed cells. Microinjection is needed when dyes are too large or cannot cross the plasma membrane. Since, there are several ways to classify and subdivided dyes, even if a dyes for that organelle exist for fixed cell, there is still a need for a dyes that stain the same organelle in a living cell.

In our laboratory, a new class of fluorescent dyes (PICs) are made using an exceedingly flexible methodology. This flexibility allows for this family of dyes to be used to study the relationships between dye structure and imaging properties inside cells.

During the course of research, several dyes were studied and their ability to cross the cellular plasma membrane was evaluated. If the dyes did cross the cellular membrane their affinity and/or selectivity properties toward specific organelles needed to be determined.

Cells and their organelles can be selectively labeled. This labeling is based on empirical testing of hundreds of different cells. Several dyes can be used to label specific organelles of living cells. The probes can be excited with multi-line lasers so the probes may be imaged simultaneously.

Confocal microscopes have optical filters that pass only selective wavelengths. When using a confocal microscope it is necessary to understand filters to process and acquire the data correctly. An excitation filter must allow passage of suitable wavelengths of light to allow excitation of the dye, yet eliminate other extraneous light. Emission filters are used to filter light exiting the sample. There are several different types of emission filters (Figure 25). They are divided according to the wavelengths of light they transmit. Long pass filters allow all wavelengths longer than their rated wavelength. A band pass filter is made by a combination of a long and a short pass filter, which allows for a narrow spectral window. The band pass width of the filter will depend on the spectral widths of the individual filters used. Being able to purchase different filters allows customization of the filters to the dyes studied in multi-channel experiments.

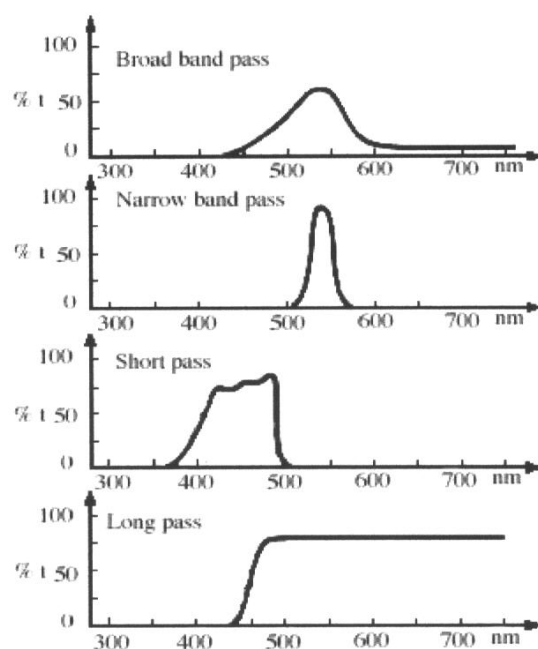


Figure 25: Optical filters for the Confocal Microscope

The utilization of fluorescent probes will certainly require the synthesis of more selective, and more intense fluorescent probes. When new dyes are developed their staining characteristics must be determined. This can be accomplished through multi-channel fluorescent (co-localization) confocal microscopy studies, which are aided by the use of different filters. Confocal microscopes have the ability to use three different filters, simultaneously. Each filter can pass a different spectral window. This allows for known and unknown dyes simultaneously detected in a cell to be monitored through different instrumental channels (filters).

For purpose of comparison Rhodamine 123 (Figure 26) and rhodamine-dextran stain mitochondria and lysosomes, respectively.¹⁸ This staining was accomplished through incubation of cells with 0.1-1 μM of rhodamine (SP) 123 for 15-30 minutes at the normal growing temperature (37.7°C). Rhodamine-dextran was incubated at 1 $\mu\text{g/ml}$ overnight.

Mitochondria therefore emitted a green fluorescent color and lysosomes emitted a red fluorescent color.¹⁹

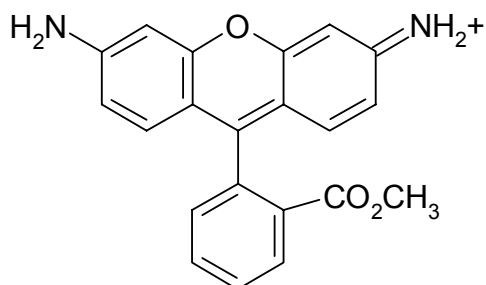


Figure 26: Rhodamine 123

Another example of co-localization is the use of ER-Tracker Blue white DPX^{®18} (Figure 27) and MitoTracker Red CM-H₂Xros^{®21} (Figure 28), which stain endoplasmic reticulum and mitochondria, respectively. The ER-Tracker Blue White DPX is a green fluorescent dye and MitoTracker Red CM-H₂Xros is red fluorescent dye. The image (Figure 29) was acquired using a fluorescent microscope using a triple-bandpass filter set appropriately for DAPI, Fluorescein, and Texas Red dyes.²¹

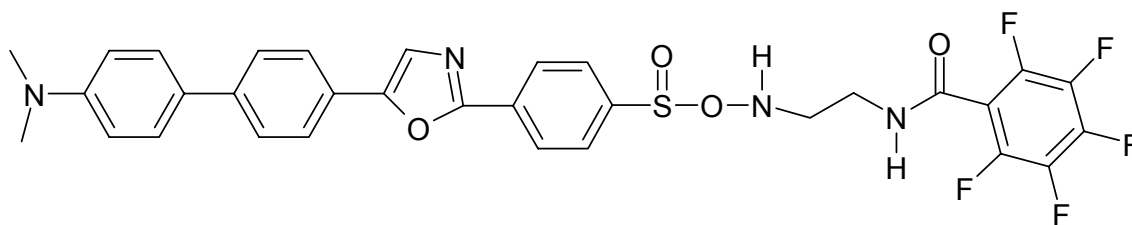


Figure 27: ER-Tracker Blue white DPX

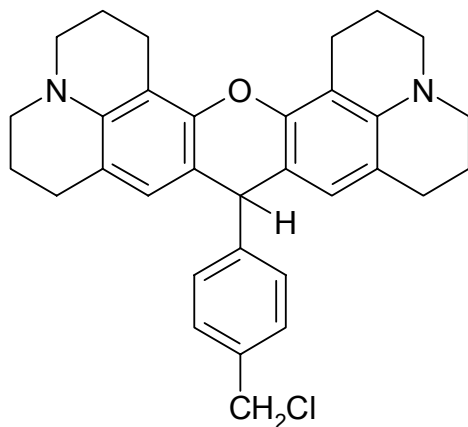


Figure 28: MitoTracker Red CM-H₂Xros

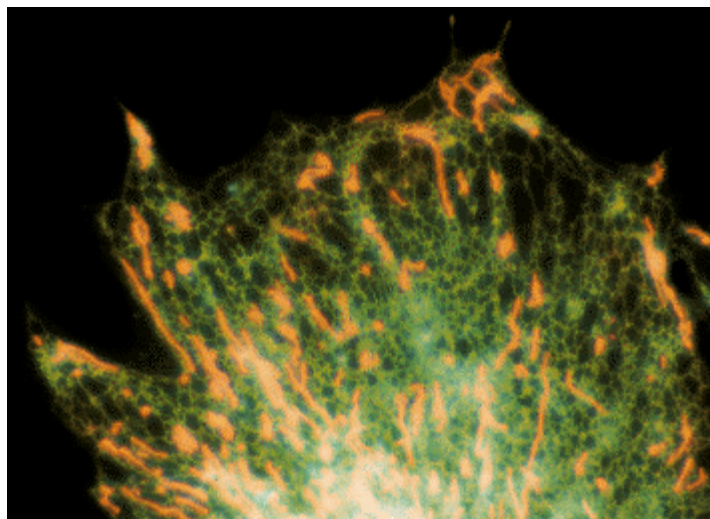


Figure 29¹⁸: Live bovine pulmonary artery endothelial cells stained with ER-Tracker Blue-White DPX and MitoTracker Red CM-H₂Xros. The endoplasmic reticulum appears green and the mitochondria appear orange.

Many other organelles have specific fluorophores designed for them.¹⁷ For example: BODIPY-ceramide derivatives (Figure 30)²⁰ and NBD-ceramide (Figure 31) are stains specific to the Golgi. Carbocyanine (Figure 32) dyes stain the endoplasmic reticulum,²¹ dihydropyrene (Figure 33) localize in the mitochondria, and the cytoskeleton can be stained selectively using Alexa Fluor 488 (Figure 34).

Phalloidin, DAPI (Figure 35) are used for staining DNA and RNA. Table 6 contains a list of potential applications for certain targeted sub cellular structure.

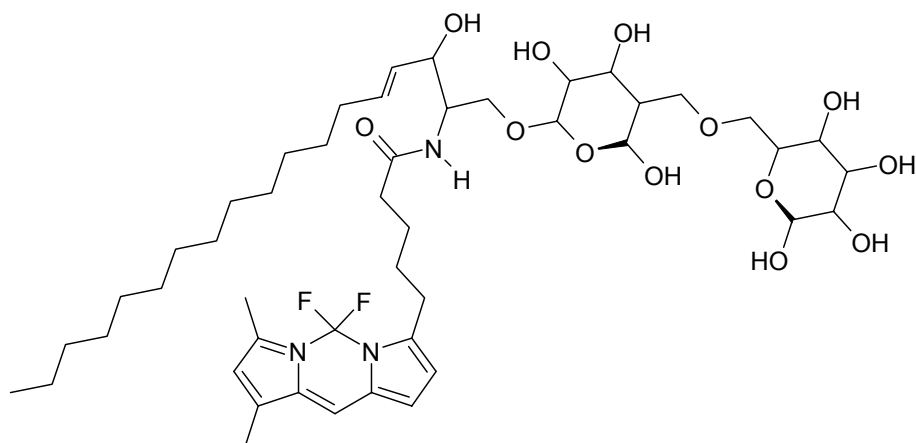


Figure 30: BODIPY-ceramide derivatives

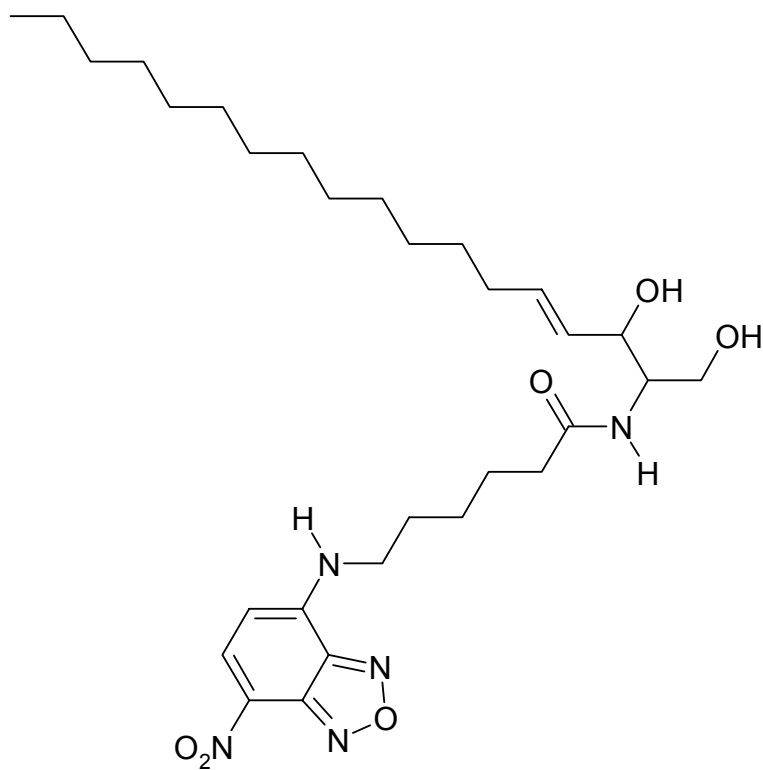


Figure 31: NBD-ceramide

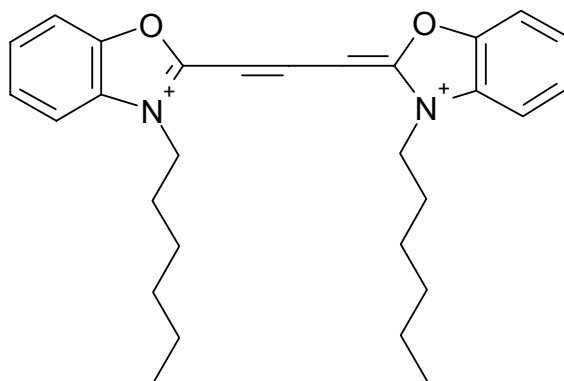


Figure 32: Carbocyanine dyes

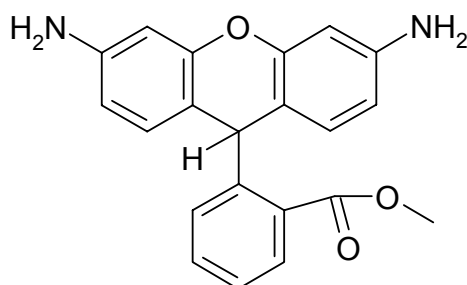


Figure 33: Dihydrorhodamine 123

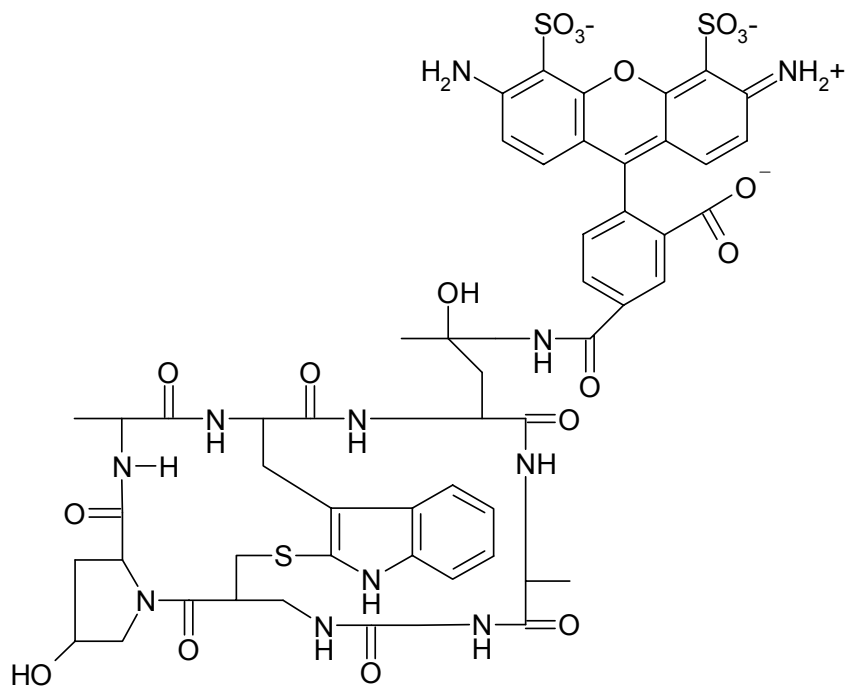


Figure 34: Alexa Fluor 488 phalloidin

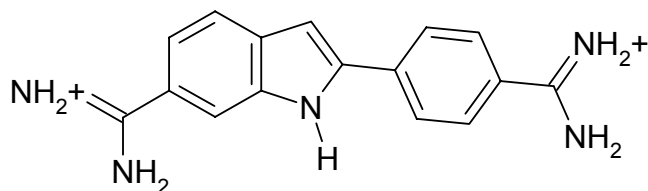


Figure 35: DAPI

Table 6²²: Sub-cellular co-localization vector for targeted organelle

Targeted sub cellular structure	Dye Colors	Localization tag or gene	Potential application
Actin filaments	Green, yellow	Human β -actin	<ul style="list-style-type: none"> study cytoskeletal dynamics monitor co-localization associated proteins or organelles
Microtubules	Green, yellow	Human α -tubulin	<ul style="list-style-type: none"> study cytoskeletal dynamics monitor co-localization associated proteins or organelles
Mitochondria	Cyan, yellow, red	Targeting sequence from subunit VIII of cytochrome c oxidase	<ul style="list-style-type: none"> study normal & disease state track mitochondrial dynamics
Nucleus	Cyan, yellow	SV40 T-antigen NLS 3 tandem repeats	<ul style="list-style-type: none"> study nuclear import track cell lineage monitor cell growth & division
Endoplasmic reticulum	Cyan, yellow	Targeting sequence of calreticulin: KDEL retrieval sequence	<ul style="list-style-type: none"> visualize tubules & cisternae track morphology & intracellular distribution
Golgi apparatus	Cyan, yellow	Targeting sequence from human beta 1: 4-galactosyltransferase	<ul style="list-style-type: none"> study organelle dynamics track morphology & intracellular distribution
Plasma membrane	Green, cyan, yellow	Palmitoylation domain of neuromodulin; farnesylation sequence from c-Ha-Ras (pEGFP-F)	<ul style="list-style-type: none"> study membrane dynamic & protrusion monitor membrane associated changes during apoptosis
Peroxisome	Green, cyan, yellow	Peroxisomal targeting signal 1 (PST1)	<ul style="list-style-type: none"> monitor movement, segregation, biogenesis & degradation study peroxisome purification

Method

The A7R5 cell line was obtained from the American Type Culture Collection and used at passage numbers 10-40. The cells were grown in Dulbecco's modified Eagles's medium (DMEM) containing 10% fetal bovine serum (FBS), 1 % penn strep. Tests for mycoplasma contamination were not performed. Cells were incubated in a humidified chamber at 37.7 °C with a mixture of 95% air and 5% carbon dioxide. Cells were grown on cover slips at 2×10^5 cells per mL for 2 days. All dyes were dissolved into a DMEM to give a concentration of 3-5 mM. Cells to be imaged were allowed to grow in this dye-containing medium for 1 hour. MitoTracker RedXros® was added at 10 mM when co-localization studies were performed. Cells were imaged on a Bio-Rad MCR 1024 Confocal Microscope. The filters used in the Microscope were: 515 long pass filter, 522/35 band pass filter and 680/32 band pass filter.

Results

The PICs **1-16** (Figure 3) used in these experiments are violet excitable green fluorescent dyes. They have excitation maximum between 390-425 nm. In all cases these positively charged dyes had no difficulty in crossing the cellular membrane without the use of DMSO. Images obtained using confocal microscopy showed dyes **1-16** (Fig 37-48) had an affinity for imaging either ER/golgi and/or mitochondria. To more definitely ascertain their staining ability inside the cells. The cells were stained with the known mitochondria stain Mitrotracker red (Figure 36) in an effort to discriminate between ER/golgi and/or mitochondria as the target organelle. Comparisons were made

between the behavior of MitoTracker red¹⁸ (Figure 36) and PICs **1-16**. Multiple dye experiments for four of these dyes were performed. Dyes **2a** (Figure 38), **1a** (Figure 40), **6a** (Figure 42), and **11b** (Figure 44) were proven to stain mitochondria through co-localization. All PICs **1-16** cross the plasma cellular membrane; they all also crossed the nuclear envelope. Dye **2a** (Figure 37), **1a** (Figure 43), and **11b** (Figure 45) revealed nuclear substructures.

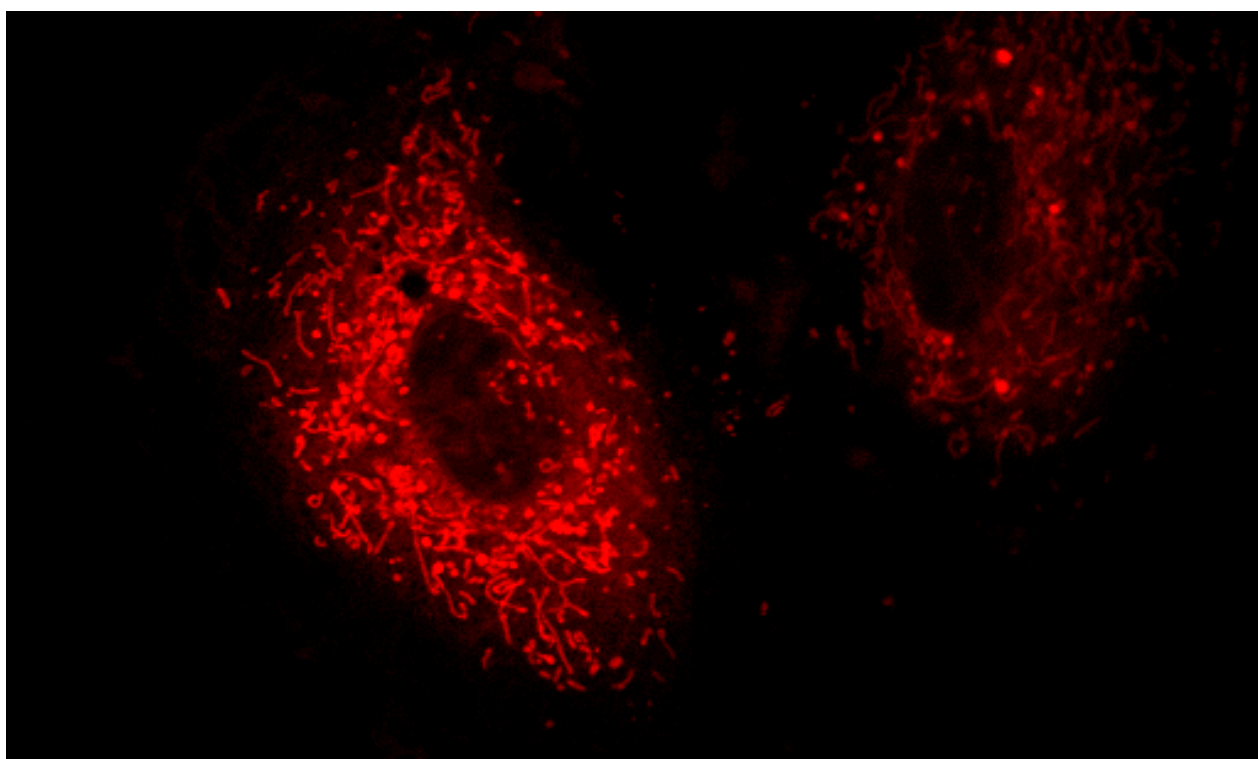


Figure 36: Mitrotracker red in A7R5

The picture in Figure 37 is of smooth muscle cells stained with dye **1a**. The small round objects appear to be the mitochondria. The objects illuminated are evenly spread out though the cell as expected for mitochondria

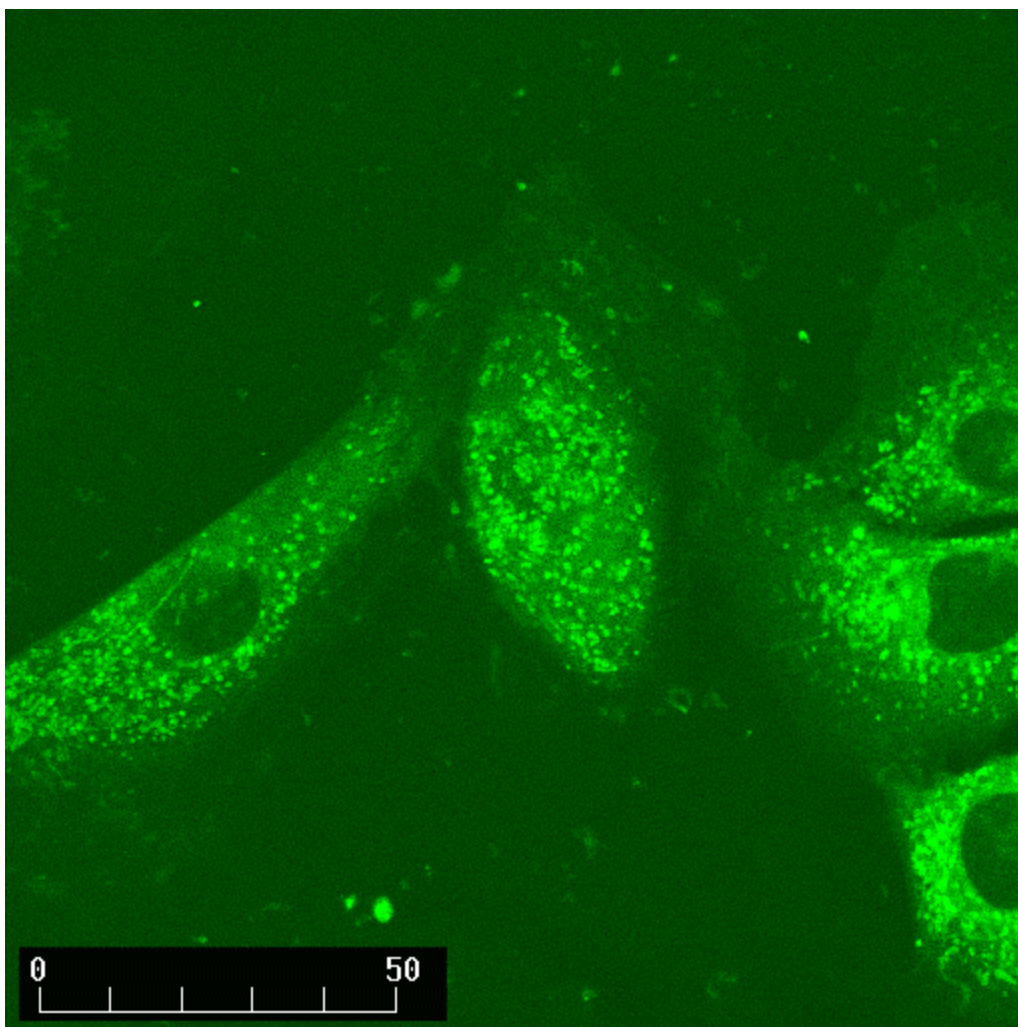


Figure 37: Dye 1a in smooth muscle cells of a rat's aorta

Co-localization studies were conducted as follows: The commercially available dye, MitoTracker red, is known to stain live mitochondria. MitoTracker red has an emission maximum at 600 nm, which was collected in one channel. PICs have emission maximum of about 525 nm, which was collected in a separate channel. The data collected in each channel is in grayscale. MitoTracker red was given a superficial blue color, while the PICs were given a superficial red color. The MitoTracker and PICs channels were overlaid. If the small object in the Figure were present in both channels it would appear purple, and if it were only in one channel it would appear blue or red

depending on the channel. Most the small round objects appear purple, which confirms that **1a** does stain mitochondria (Figure 38). The objects in the nucleolus are stained from **1a**.

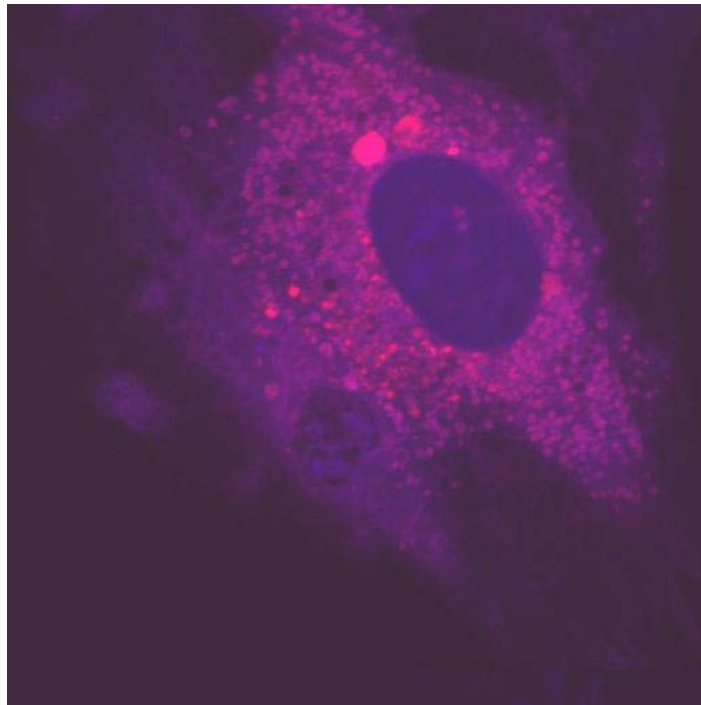


Figure 38: Dye 1a and MitoTracker red in smooth muscle cells of a rat's aorta

The picture in Figure 39 is of smooth muscle cells stained with dye **11b**. It appears as though the relatively large football shape objects might be mitochondria along with the long strand structures.

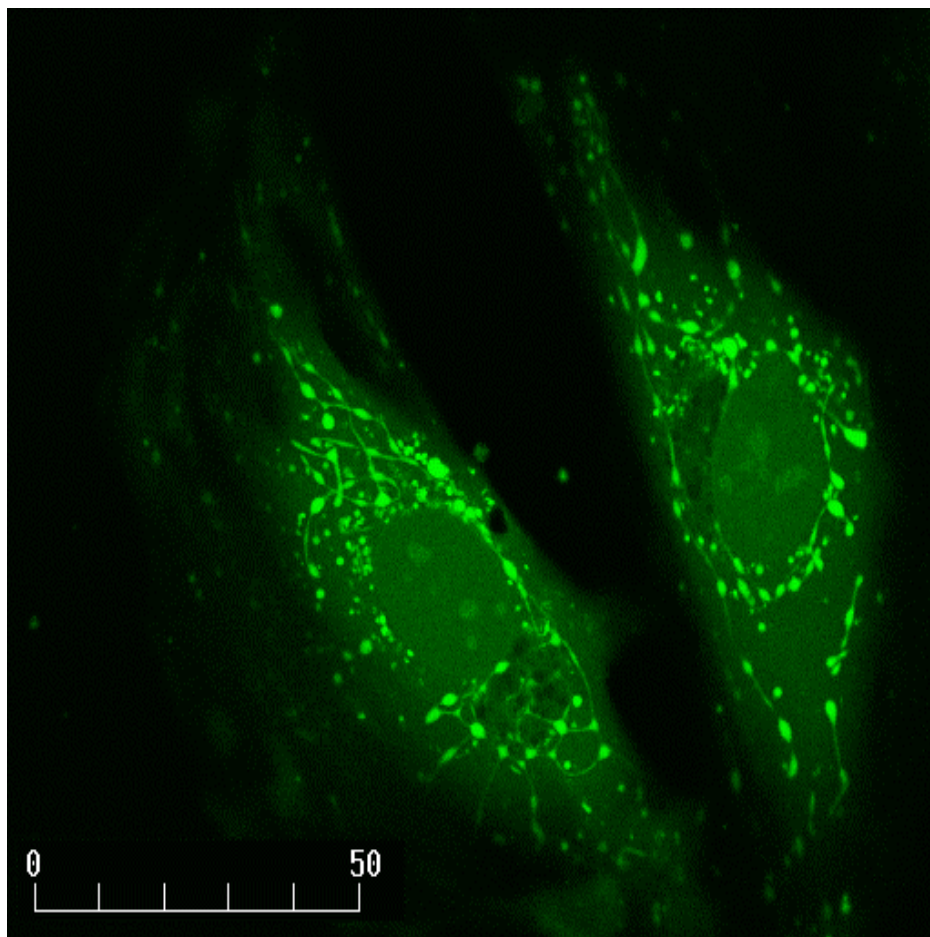


Figure 39: Dye 2a in smooth muscle cells of a rat's aorta

The same method for co-localization was used as described above. Most of the small round objects appear purple, which confirms that dye **11b** does stain mitochondria (Figure 40).

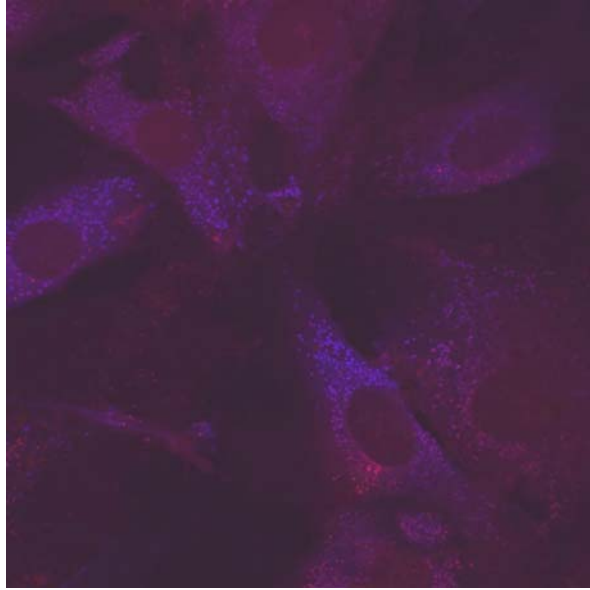


Figure 40: Dye 2a and MitoTracker red in smooth muscle cells of a rat's aorta

The picture in Figure 41 is of smooth muscle cells stained with dye **1e**. Long strand-like objects are thought to be mitochondria.

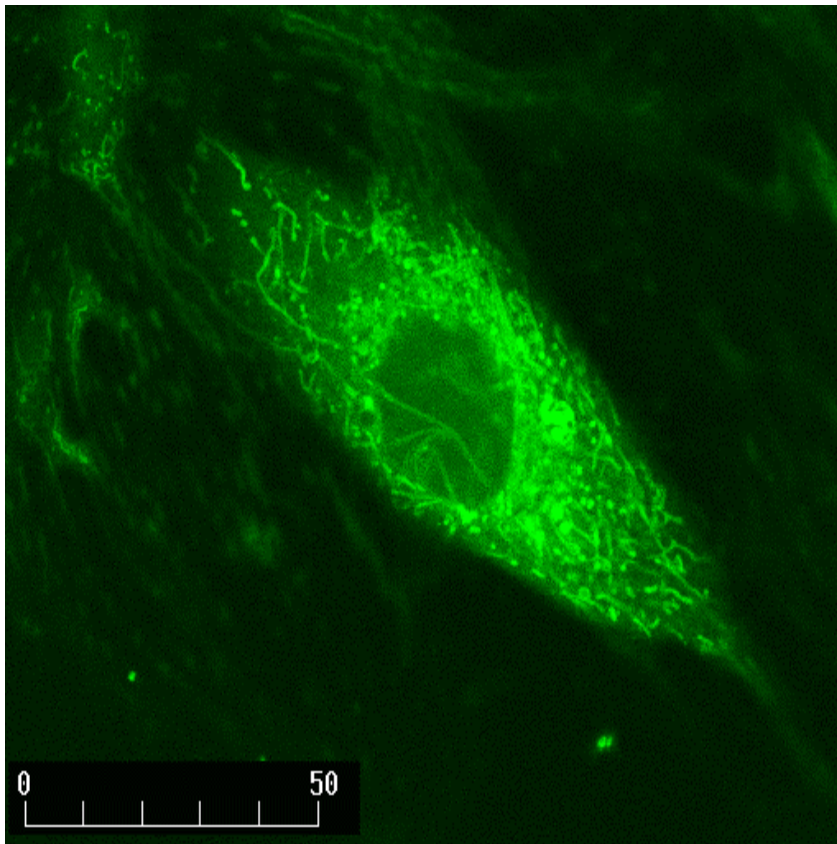


Figure 41: Dye 1e in smooth muscle cells of a rat's aorta

The same method for co-localization in smooth muscle cells of a rat's aorta was used as described above. The small round objects appear purple, which confirms that dye **6a** does stain mitochondria in Figure 42

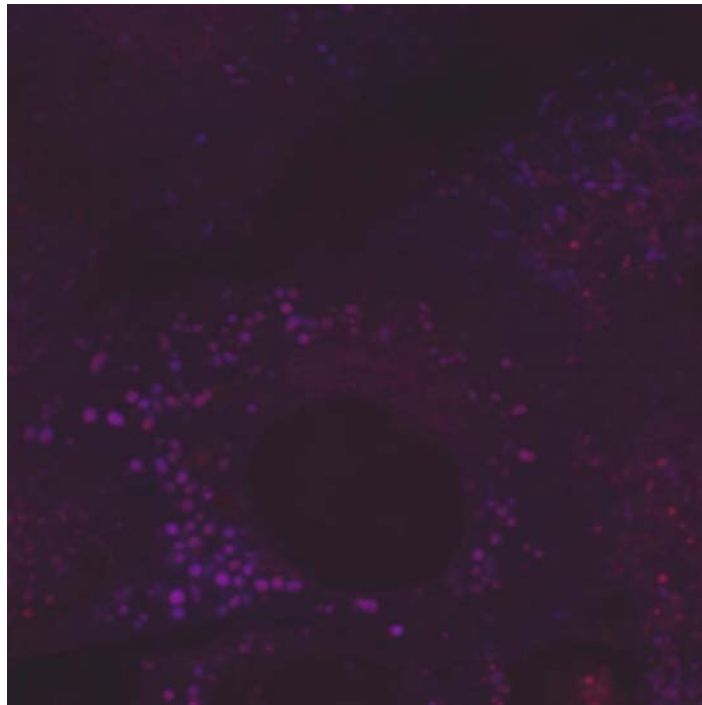


Figure 42: Dye 1e and MitoTracker red in smooth muscle cells of a rat's aorta

The picture in Figure 43 is of smooth muscle cells stained with dye **2a**. The long strand structures are thought to be mitochondria. The long strands are evenly spread out though the cell, as mitochondria should appear. The mitochondria brightness is much higher than the background.

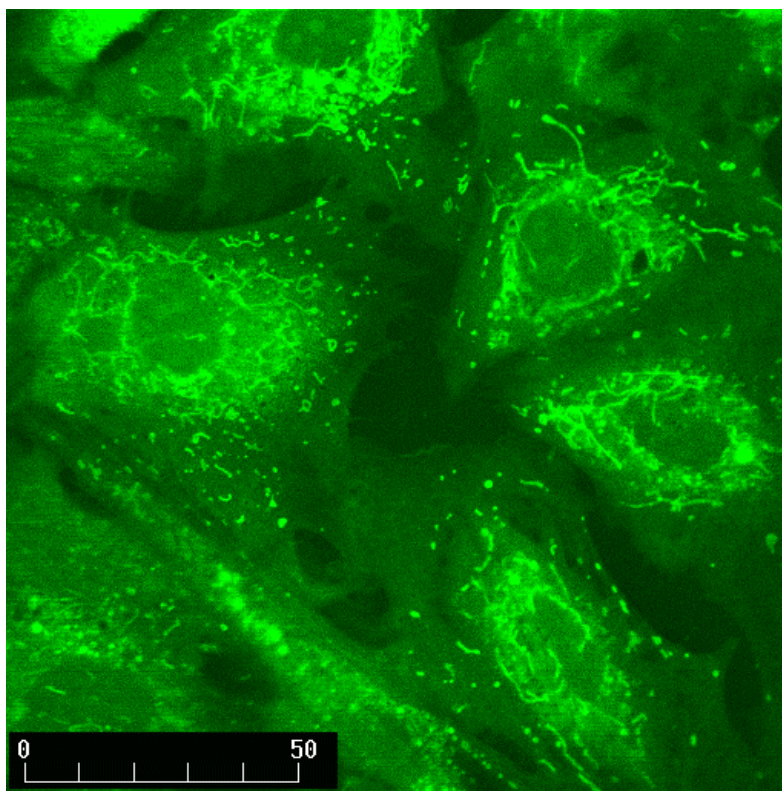


Figure 43: Dye 1b in smooth muscle cells of a rat's aorta

The same method for co-localization in smooth muscle cells of a rat's aorta was used as described above. Most the small round objects appear purple, which confirms that dye **2a** does stain mitochondria Figure 44

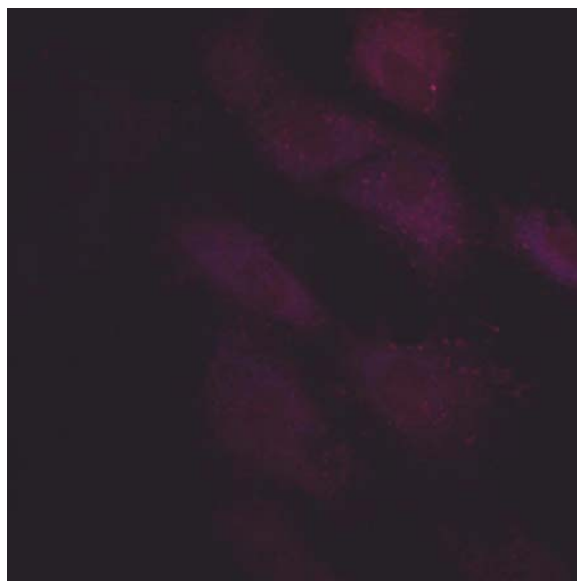


Figure 44: Dye 1b & MitoTracker red in smooth muscle cells of a rat's aorta

The picture in Figure 45 is of smooth muscle cells stained with dye **6a**. The long strand-like structures are thought to be mitochondria.

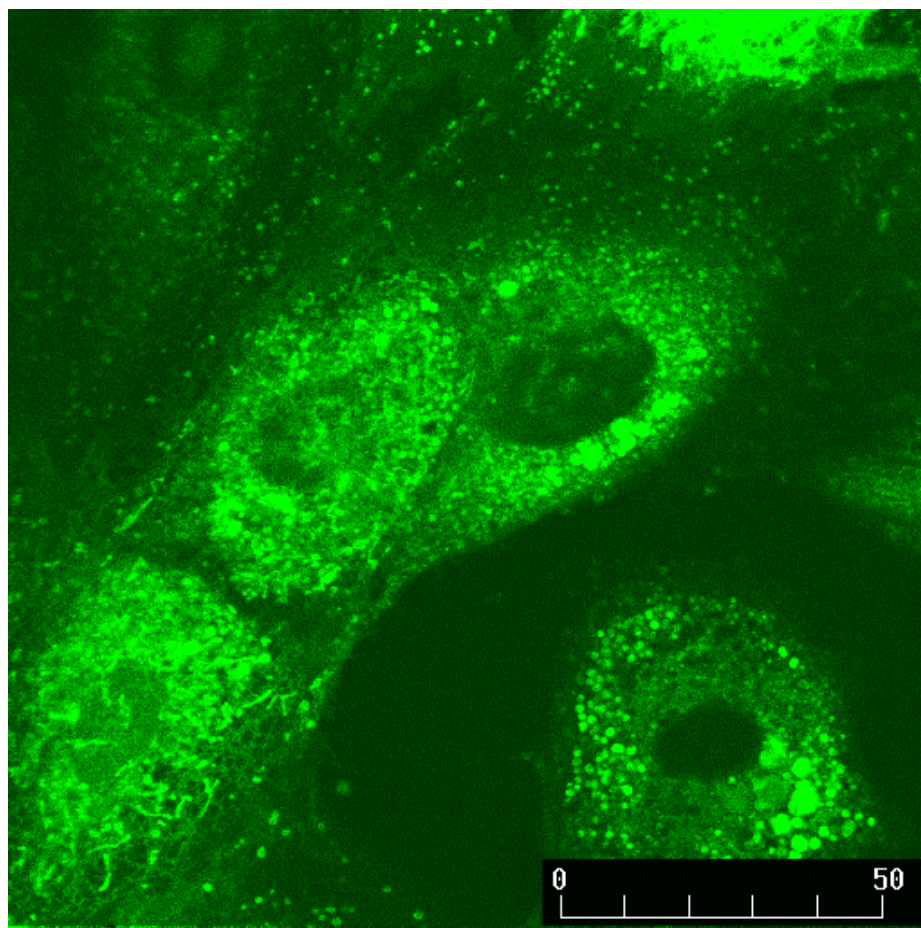


Figure 45: Dye 2e in smooth muscle cells of a rat's aorta

Dyes that are specific for nuclear envelopes are uncommon (lucifer yellow). The flexible methodology for synthesizing dyes allows for charge/structure relationships. Dyes **13b** (Figure 46) and **14b** (Figure 47) appeared to stain the nuclear envelope of the cells. Tri-cationic **14b** seems to have no difficulty crossing the plasma membrane and localizing in the nuclear envelope. Also interesting, dyes **13b** and **14b** are very similar in

structure, but are different in their charge (**13b** +1, **14b** +3). This would indicate that staining the nuclear envelopes in live cells is not charge dependent but structure dependent.

Dyes that are specific for nuclear envelopes in fixed cells are uncommon, but those that staining nuclear envelopes in live cells are rare. Once the dyes were proven to stain the nuclear envelope it was important to prove that the cells stained with **13b** were still viable. Two methods were used, which were staining with 4% trypan blue²³ and MitoTracker Red CM-H2Xros.¹⁸ Trypan blue has no effect on living cells but renders dead cells or cells with a damaged cell membrane blue, as observed with an optical microscope. After 5 minutes, the cells were still colorless, demonstrating that they were neither damaged nor dead. MitoTracker Red CM-H2Xros is a non-luminescent stain, which will only fluoresce after being oxidized by the mitochondria, it then becomes a red fluorescent dye with an emission maximum at 600 nm. Emission at 600 nm was observed with MitoTracker Red CM-H2Xros stained cells, also indicating their vitality. To our knowledge dye **14b** is the first red fluorescent dye which stained the nuclear envelope in live cells. This ability to stain the nuclear envelope would be of great interest in co-staining live cells with other dyes. This dye may have uses in plant cells.

The picture in Figure 46 is of smooth muscle cells stained with dye **14b**. Dye **14b** specific stains nuclear envelope.

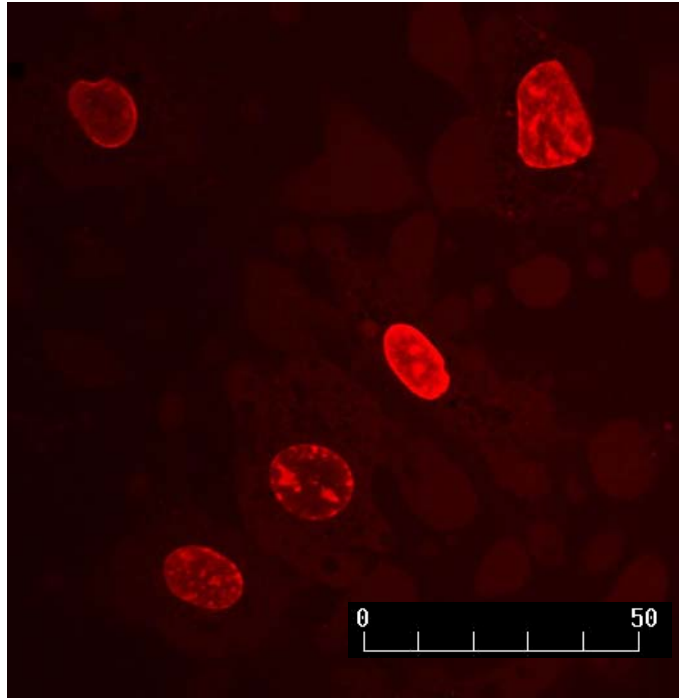


Figure 46: Dye 2d in smooth muscle cells of a rat's aorta

The picture in Figure 47 is of smooth muscle cells stained with dye **13b**. Dye **14b** seems to locate around the nuclear envelope, although there are is dye in the cytoplasm.

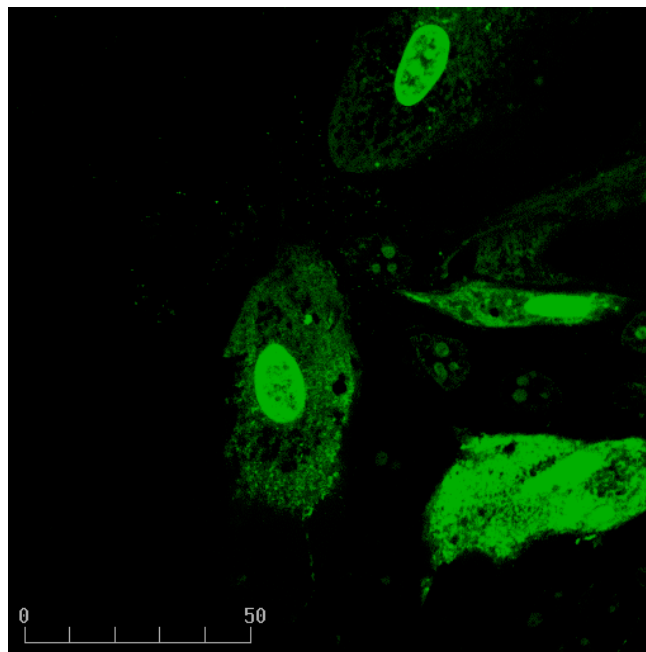


Figure 47: Dye 2c in smooth muscle cells of a rat's aorta

Conclusion

The behavior of green fluorescent PICs in live smooth muscle cells was probed using confocal microscopy. Dyes **2a**, **1a**, **6a**, and **11b** were proven to stain mitochondria through co-localization. All PICs 1 and 2 cross the plasma cellular membrane, they all also crossed the nuclear envelope. Dye **2a**, **1a**, and **11b** revealed nuclear substructures. Dyes **13b** and **14b** are very similar in structure, but are different in their charge (**13b** +1, **14b** +3). This would indicate that staining the nuclear envelopes in live cells is structure dependent not charge dependent. To our knowledge dye **14b** is the first red fluorescent dye that has been shown to stain the nuclear envelope in live cells.

Chapter 4: Summary and Conclusion

Pyridoimidazolium cations (PICs) are a new class of fluorescent dyes, which are prepared by an exceedingly flexible methodology. Using computational chemical methods the excitation and emission maxima of these dyes were simulated. This was best accomplished through geometry optimization (MM+) followed by calculating the electronic spectra with ZINDO/S. This protocol has been found to be effective and has the potential to greatly streamline the design of new longer wavelength dyes. New longer wavelength dyes have now been identified as synthetic targets, **16b**.

The presences of amino groups on a known fluorescent ring system are well established to markedly affect the optical properties of the dye. Methodology had been developed for the amination of different position on the 2-(2-pyridyl)-carboxyquinoline ring system(4-Carboxymethyl-6-amino-2-(2-pyridyl)quinoline,**8a**, and 4-Carboxymethyl-8-amino-2-(2-pyridyl)quinoline), leading to the testing of three new amino substituted fluorescent dyes. Another methodology was effect in synthesis of 4-amino-2-(2-pyridyl)quinoline, **6a**. This is also the precursor to 4-isothiocyanato-amino-2-(2-pyridyl)quinoline, which can be used as a cellular tag for proteins.

The behavior of green fluorescent PICs in live smooth muscle cells, was probed using confocal microscopy. Dyes **2a**, **1a**, **6a**, and **11b** were proven to stain mitochondria through co-localization. All PICs 1 and 2 cross the plasma cellular membrane, they all also crossed the nuclear envelope. Dye **2a**, **1a**, and **11b** revealed nuclear substructures. Dyes **13b** and **14b** are very similar in structure, but are different in their charge (**13b** +1,

14b +3). This would indicate that staining the nuclear envelopes in live cells is structure dependent not charge dependent. To our knowledge dye **14b** is the first red fluorescent dye that has been shown to stain the nuclear envelope in live cells.

-
- 1 Donovan R.J. and Morgan R.J.; U.S. Patent 5,874,587 Feb. 23, 1999
 - 2 Walkup, Grant; Burdette, Shawn; Lippard, Stephan; Tsien, Roger; *J. Am. Chem. Soc.* **2000**, *122* 6544-5645
 - 3 Walkup, Grant; Burdette, Shawn; Lippard, Stephan; Tsien, Roger, *J. Am. Chem. Soc.* **2001**, *123*, 7831-7841
 - 4 Clark, Tim, *A handbook of Computational Chemistry*; John Wiley and Sons, 1985
 - 5 Foresman, James, Frisch Elen, "Exploring Chemistry with Electronic Structure Methods; Gaussian, Inc: Pittsburg, PA, 1996
 - 6 Fabian W. M.F., *Journal of Molecular Structure* **1999** *477* 209-220
 - 7 R.S. Becker, S. Chakravorti, C.A. Garnter, M. de Graca Miguel; *J. Chem., Faraday Trans.* **1993** *89* 1007
 - 8 U. Brackmann, *Lambdachrome Laser Dyes*; Lambda Physik GmbH: Gottingen, 1986
 - 9 Snavely B. B., Birks J.B., *Organic Molecular Photo Physics*; John Wiley and Sons: London, England, 1973, Chapter 5
 - 10 Reynolds G.A., Drexhage K.H., *Opt. Commun.* **1975** *47* 222
 - 11 Fletcher A.N., Bliss D.E., J.M. Kauffman, *Opt. Commun.* **1983** *47* 57
 - 12 *ISIS draw software*, <http://www.mdli.com/downloads/free.html/> (accessed 4/25/02)
 - 13 Newkome, George.; Gross, Jens.; Patri, Anil; *J. Org. Chem.* **1997**, *62*, 3013-3014
 - 14 Hawthorne, Frederick; Thompson, Michael; Mizusawa, Eugene; *Inorg. Chem.* **1985**, *24*, 1911-1916
 - 15 Fluorescent Microscopy, Bangle, Robert, Jr [http:// glinda.lrsn.upenn.edu/~weeks/confocal/](http://glinda.lrsn.upenn.edu/~weeks/confocal/) (accessed 5/27/02)
 - 16 Wang, Herman, *Fluorescence Imaging Spectroscopy and Microscopy*; John Wiley & Sons, Inc. 1996
 - 17 Molecular Probes, Eugene Oregon. www.probes.com/ (accessed 4/28/02)
 - 18 Goeres, Johnson, *J. Cell. Biol.* **1981** *88* 526-535
 - 19 Lemasters, Diguiseppi, Nieminen, Herman, B. *Laser scanning confocal microscopy of living cells, Optical Microscopy: Emerging Methods and Applications*; Academic Press: New York, NY; 1993 pp 339-354
 - 20 Pagano R. E., Martin, O.D., Kang, H.C., Haugland, R.P. *J. Cell. Biol.* **1991** *113* 1267-1279
 - 21 Lee, C., Chen, L. B. *Dynamic behavior of endoplasmic reticulum in living cells*. Cell: Cambridge, Ma. 1988 37-46
 - 22: Clontech, <http://www.probes/clontech.com/> (accessed 4/21/02)
 - 23 Sigma-Aldrich <http://www.sigma-aldrich.com/> (accessed 5/25/02)

Appendix I

```
HyperChem log start -- Mon Jul 01 20:43:36 2002.
Geometry optimization, MolecularMechanics, molecule = C:\My
Documents\Hyper chem files\cincacid.hin.
mmplus
PolakRibiere optimizer
Default parameters being used for torsions...
Default parameters being used for bends...
Energy=25.515825 Gradient=0.092821 Converged=YES (0 cycles 1 points).
Bond=1.84261 Angle=19.4408 Dihedral=-6.27828 Vdw=17.6903 Stretch-
bend=0.286719 Electrostatic=-7.46631.
Single Point, SemiEmpirical, molecule = C:\My Documents\Hyper chem
files\cincacid.hin.
ZINDOS
Convergence limit = 0.0100000 Iteration limit = 50
Overlap weighting factors: P(Sigma-Sigma) = 1.2670 and P(Pi-Pi) =
0.5850
Accelerate convergence = YES
RHF Calculation:

Singlet state calculation
Configuration interaction will be used
Number of electrons = 114
Number of Double Occupied Levels = 57
Charge on the System = 1
Total Orbitals = 108
Number of Occupied Orbitals Used in CI = 5
Number of Unoccupied Orbitals Used in CI = 5

Starting ZINDO/S calculation with 108 orbitals

Iteration = 1 Difference = 67452.50648
Iteration = 2 Difference = 375.77163
Iteration = 3 Difference = 34.03356
Iteration = 4 Difference = 19.82689
Iteration = 5 Difference = 24.72793
Iteration = 6 Difference = 0.28406
Iteration = 7 Difference = 0.10147
Iteration = 8 Difference = 0.01821
Iteration = 9 Difference = 0.00683
Starting a singly excited CI calculation with 51 configurations.
Computing the integrals for CI matrix: done 0%.
Computing the integrals for CI matrix: done 10%.
Computing the integrals for CI matrix: done 20%.
Computing the integrals for CI matrix: done 30%.
Computing the integrals for CI matrix: done 40%.
Computing the integrals for CI matrix: done 50%.
Computing the integrals for CI matrix: done 60%.
Computing the integrals for CI matrix: done 70%.
Computing the integrals for CI matrix: done 80%.
Computing the integrals for CI matrix: done 90%.
Computing the integrals for CI matrix: done 100%.
Computing the CI matrix...
Diagonalizing the CI matrix...
```

Computing the properties of the CI states...

***** UV Spectrum *****

---- Absolute Energy in eV.

---- Dipole Moments in Debye.

0 (Reference) Absolute Energy -4439.31592

1 Spin S 0.00
State Dipole 7.8538

State Dipole Components 7.2633 -2.9508 -

0.4692

1 (Transition) Excitation Energy 921.8 nm
10848.4 1/cm

1 -> 2 Spin S 1.00
State Dipole 9.3690
Oscillator Strength 0.0000

State Dipole Components 8.9026 -2.8550 -0.6081
Transition Dipole Components -0.0000 0.0000 0.0000

Spin Up : Occ. MO --> Unocc. MO Coefficients

57 --> 58 0.658679

Spin Down: Occ. MO --> Unocc. MO Coefficients

57 --> 58 0.658679

2 (Transition) Excitation Energy 670.1 nm
14922.6 1/cm

1 -> 3 Spin S 1.00
State Dipole 5.2560
Oscillator Strength 0.0000

State Dipole Components 3.6432 -3.7866 -0.1222
Transition Dipole Components 0.0000 -0.0000 0.0000

Spin Up : Occ. MO --> Unocc. MO Coefficients

57 --> 59 -0.574307

Spin Down: Occ. MO --> Unocc. MO Coefficients

57 --> 59 -0.574307

3 (Transition) Excitation Energy 519.1 nm
 19263.5 1/cm

1 -> 4 Spin S 1.00
 State Dipole 7.6766
 Oscillator Strength 0.0000

 State Dipole Components 4.6532 -6.1048 -0.0902
 Transition Dipole Components 0.0000 0.0000 -0.0000

Spin Up : Occ. MO --> Unocc. MO Coefficients

 57 --> 60 -0.550858

Spin Down: Occ. MO --> Unocc. MO Coefficients

 57 --> 60 -0.550858

4 (Transition) Excitation Energy 433.7 nm
 23058.5 1/cm

1 -> 5 Spin S 0.00
 State Dipole 9.0062
 Oscillator Strength 0.7163

 State Dipole Components 7.3561 -5.1835 -0.3612
 Transition Dipole Components 8.0882 -0.4876 -0.6383

Spin Up : Occ. MO --> Unocc. MO Coefficients

 57 --> 58 0.691536

Spin Down: Occ. MO --> Unocc. MO Coefficients

 57 --> 58 -0.691536

5 (Transition) Excitation Energy 409.4 nm
 24428.8 1/cm

1 -> 6 Spin S 1.00
 State Dipole 7.0557
 Oscillator Strength 0.0000

 State Dipole Components 5.8033 -4.0018 -0.2994
 Transition Dipole Components 0.0000 0.0000 -0.0000

Spin Up : Occ. MO --> Unocc. MO Coefficients

 56 --> 58 0.408779

Spin Down: Occ. MO --> Unocc. MO Coefficients			

	56	-->	58 0.408779
6 (Transition) Excitation Energy 394.4 nm			
25354.1 1/cm			
1 ->	7	Spin S	0.00
		State Dipole	8.0368
		Oscillator Strength	0.1752
State Dipole Components 7.0122 -3.9071 -0.3929			
Transition Dipole Components -2.0240 -3.2373 0.3433			
Spin Up : Occ. MO --> Unocc. MO Coefficients			

	57	-->	59 0.648244
Spin Down: Occ. MO --> Unocc. MO Coefficients			

	57	-->	59 -0.648244
7 (Transition) Excitation Energy 372.8 nm			
26825.0 1/cm			
1 ->	8	Spin S	1.00
		State Dipole	8.5066
		Oscillator Strength	0.0000
State Dipole Components 8.2335 -2.0550 -0.5909			
Transition Dipole Components 0.0000 0.0000 -0.0000			
Spin Up : Occ. MO --> Unocc. MO Coefficients			

	57	-->	61 -0.548251
	55	-->	59 -0.337136
Spin Down: Occ. MO --> Unocc. MO Coefficients			

	57	-->	61 -0.548251
	55	-->	59 -0.337136
8 (Transition) Excitation Energy 335.7 nm			
29788.7 1/cm			
1 ->	9	Spin S	1.00
		State Dipole	10.4357
		Oscillator Strength	0.0000
State Dipole Components 9.3946 -4.5070 -0.5766			
Transition Dipole Components -0.0000 -0.0000 0.0000			
Spin Up : Occ. MO --> Unocc. MO Coefficients			

	56	-->	58 -0.387314

		55	-->	58	0.441698			
	Spin Down:	Occ. MO	-->	Unocc. MO	Coefficients			
		56	-->	58	-0.387314			
		55	-->	58	0.441698			
9	(Transition)	Excitation Energy			326.4 nm			
					30639.1 1/cm			
	1 ->	10	Spin S		0.00			
			State Dipole		5.5655			
			Oscillator Strength		0.0061			
			State Dipole Components	3.0015	-4.6867	-0.0302		
			Transition Dipole Components	-0.3873	0.5223	0.0038		
	Spin Up :	Occ. MO	-->	Unocc. MO	Coefficients			
		57	-->	60	-0.667004			
	Spin Down:	Occ. MO	-->	Unocc. MO	Coefficients			
		57	-->	60	0.667004			
10	(Transition)	Excitation Energy			326.2 nm			
					30658.3 1/cm			
	1 ->	11	Spin S		1.00			
			State Dipole		5.9428			
			Oscillator Strength		0.0000			
			State Dipole Components	-2.8240	5.2289	-0.0360		
			Transition Dipole Components	0.0000	0.0000	0.0000		
	Spin Up :	Occ. MO	-->	Unocc. MO	Coefficients			
		53	-->	58	-0.604259			
	Spin Down:	Occ. MO	-->	Unocc. MO	Coefficients			
		53	-->	58	-0.604259			
11	(Transition)	Excitation Energy			323.0 nm			
					30957.7 1/cm			
	1 ->	12	Spin S		1.00			
			State Dipole		8.8837			
			Oscillator Strength		0.0000			
			State Dipole Components	5.1165	-7.2618	-0.0854		
			Transition Dipole Components	0.0000	-0.0000	-0.0000		

Spin Up : Occ. MO --> Unocc. MO Coefficients						

	56	-->	59		0.494328	
	56	-->	61		0.365019	
Spin Down: Occ. MO --> Unocc. MO Coefficients						

	56	-->	59		0.494328	
	56	-->	61		0.365019	
12 (Transition)	Excitation Energy			313.3 nm		
				31916.3 1/cm		
1 -> 13	Spin S		0.00			
	State Dipole		6.0425			
	Oscillator Strength		0.0002			
	State Dipole Components		-2.9240	5.2878	-0.0308	
	Transition Dipole Components		-0.0132	0.0106	-0.1142	
Spin Up : Occ. MO --> Unocc. MO Coefficients						

	53	-->	58		-0.609937	
Spin Down: Occ. MO --> Unocc. MO Coefficients						

	53	-->	58		0.609937	
13 (Transition)	Excitation Energy			300.6 nm		
				33261.7 1/cm		
1 -> 14	Spin S		0.00			
	State Dipole		6.9091			
	Oscillator Strength		0.4343			
	State Dipole Components		4.6467	-5.1107	-0.1564	
	Transition Dipole Components		-3.3867	-4.0068	0.4930	
Spin Up : Occ. MO --> Unocc. MO Coefficients						

	57	-->	61		-0.411881	
	56	-->	58		0.422232	
Spin Down: Occ. MO --> Unocc. MO Coefficients						

	57	-->	61		0.411881	
	56	-->	58		-0.422232	
14 (Transition)	Excitation Energy			299.2 nm		
				33425.1 1/cm		
1 -> 15	Spin S		1.00			
	State Dipole		11.3815			
	Oscillator Strength		0.0000			
	State Dipole Components		9.1455	-6.7628	-0.4028	
	Transition Dipole Components		0.0000	0.0000	-0.0000	
Spin Up : Occ. MO --> Unocc. MO Coefficients						

	57	-->	62	-0.405065
	55	-->	58	-0.351218
Spin Down:	Occ. MO	-->	Unocc. MO	Coefficients

	57	-->	62	-0.405065
	55	-->	58	-0.351218
15 (Transition)	Excitation Energy	298.3 nm		
		33527.3 1/cm		
1 ->	16	Spin S	1.00	
		State Dipole	16.3314	
		Oscillator Strength	0.0000	
		State Dipole Components	11.9267	-11.1524 -0.3036
		Transition Dipole Components	0.0000	0.0000 -0.0000
Spin Up :	Occ. MO	-->	Unocc. MO	Coefficients

	54	-->	58	0.461115
	54	-->	59	0.403452
Spin Down:	Occ. MO	-->	Unocc. MO	Coefficients

	54	-->	58	0.461115
	54	-->	59	0.403452
16 (Transition)	Excitation Energy	297.3 nm		
		33635.6 1/cm		
1 ->	17	Spin S	0.00	
		State Dipole	17.1313	
		Oscillator Strength	0.0047	
		State Dipole Components	12.1779	-12.0471 -0.2198
		Transition Dipole Components	-0.3060	-0.4515 0.0197
Spin Up :	Occ. MO	-->	Unocc. MO	Coefficients

	54	-->	58	0.490264
	54	-->	59	0.426896
Spin Down:	Occ. MO	-->	Unocc. MO	Coefficients

	54	-->	58	-0.490264
	54	-->	59	-0.426896
17 (Transition)	Excitation Energy	293.2 nm		
		34101.1 1/cm		
1 ->	18	Spin S	0.00	
		State Dipole	9.3148	

	Oscillator Strength	0.0085			
	State Dipole Components	3.7398	-8.5307	0.0758	
	Transition Dipole Components	0.0995	-0.7225	0.0216	
Spin Up : Occ. MO --> Unocc. MO Coefficients					

	56 -->	58		0.393011	
	55 -->	58		0.428684	
Spin Down: Occ. MO --> Unocc. MO Coefficients					

	56 -->	58		-0.393011	
	55 -->	58		-0.428684	
18 (Transition)	Excitation Energy	277.5 nm			
		36033.5 1/cm			
1 -> 19	Spin S	1.00			
	State Dipole	7.9001			
	Oscillator Strength	0.0000			
	State Dipole Components	7.1327	-3.3680	-0.4393	
	Transition Dipole Components	-0.0000	-0.0000	0.0000	
Spin Up : Occ. MO --> Unocc. MO Coefficients					

	57 -->	61		-0.350414	
	55 -->	59		0.481186	
Spin Down: Occ. MO --> Unocc. MO Coefficients					

	57 -->	61		-0.350414	
	55 -->	59		0.481186	
19 (Transition)	Excitation Energy	273.6 nm			
		36551.6 1/cm			
1 -> 20	Spin S	0.00			
	State Dipole	11.9409			
	Oscillator Strength	0.3367			
	State Dipole Components	11.6706	-2.3730	-0.8674	
	Transition Dipole Components	0.5430	4.3842	-0.2675	
Spin Up : Occ. MO --> Unocc. MO Coefficients					

	57 -->	61		-0.365808	
	55 -->	58		0.486533	
Spin Down: Occ. MO --> Unocc. MO Coefficients					

	57 -->	61		0.365808	
	55 -->	58		-0.486533	
20 (Transition)	Excitation Energy	265.6 nm			
		37655.9 1/cm			

1 -> 21	Spin S	-0.00		
	State Dipole	12.6826		
	Oscillator Strength	0.1952		
	State Dipole Components	12.4304	-2.3425	-0.9204
	Transition Dipole Components	3.3018	-0.2322	-0.2606
Spin Up : Occ. MO --> Unocc. MO Coefficients				

	57 --> 62	0.488568		
	56 --> 59	-0.342710		
Spin Down: Occ. MO --> Unocc. MO Coefficients				

	57 --> 62	-0.488568		
	56 --> 59	0.342710		
21 (Transition)	Excitation Energy	258.4 nm		
		38706.6 1/cm		
1 -> 22	Spin S	1.00		
	State Dipole	10.3085		
	Oscillator Strength	0.0000		
	State Dipole Components	8.6672	-5.5621	-0.4571
	Transition Dipole Components	-0.0000	-0.0000	0.0000
Spin Up : Occ. MO --> Unocc. MO Coefficients				

	56 --> 62	0.497894		
Spin Down: Occ. MO --> Unocc. MO Coefficients				

	56 --> 62	0.497894		
22 (Transition)	Excitation Energy	250.4 nm		
		39931.0 1/cm		
1 -> 23	Spin S	0.00		
	State Dipole	6.0891		
	Oscillator Strength	0.6878		
	State Dipole Components	2.3728	-5.6074	0.0607
	Transition Dipole Components	-5.9351	-1.0639	0.5247
Spin Up : Occ. MO --> Unocc. MO Coefficients				

	56 --> 59	0.518637		
	55 --> 59	-0.342089		
Spin Down: Occ. MO --> Unocc. MO Coefficients				

	56 --> 59	-0.518637		
	55 --> 59	0.342089		
23 (Transition)	Excitation Energy	244.8 nm		
		40847.3 1/cm		

```

1 -> 24 Spin S              1.00
      State Dipole          12.8386
      Oscillator Strength    0.0000
      State Dipole Components 2.0462 -12.6630 0.5415
      Transition Dipole Components -0.0000 -0.0000 0.0000

Spin Up :  Occ. MO  -->  Unocc. MO  Coefficients
-----
          55 -->    60          -0.360460
          54 -->    58          -0.333624

Spin Down:  Occ. MO  -->  Unocc. MO  Coefficients
-----
          55 -->    60          -0.360460
          54 -->    58          -0.333624

24 (Transition) Excitation Energy      244.2 nm
                                      40946.6 1/cm

1 -> 25 Spin S              1.00
      State Dipole          13.9802
      Oscillator Strength    0.0000
      State Dipole Components 3.0993 -13.6234 0.4935
      Transition Dipole Components 0.0000 0.0000 0.0000

Spin Up :  Occ. MO  -->  Unocc. MO  Coefficients
-----
          55 -->    60           0.337826
          54 -->    58          -0.368394

Spin Down:  Occ. MO  -->  Unocc. MO  Coefficients
-----
          55 -->    60           0.337826
          54 -->    58          -0.368394

25 (Transition) Excitation Energy      244.1 nm
                                      40964.7 1/cm

1 -> 26 Spin S              0.00
      State Dipole          19.7618
      Oscillator Strength    0.0020
      State Dipole Components 8.7107 -17.7351 0.3464
      Transition Dipole Components -0.0333 -0.3092 -0.0790

Spin Up :  Occ. MO  -->  Unocc. MO  Coefficients
-----
          54 -->    58          -0.492916
          54 -->    59           0.391990

Spin Down:  Occ. MO  -->  Unocc. MO  Coefficients
-----
          54 -->    58           0.492916
          54 -->    59          -0.391990

```

26 (Transition) Excitation Energy 242.4 nm
 41259.3 1/cm

1 -> 27 Spin S 0.00
 State Dipole 7.6399
 Oscillator Strength 0.3868
 State Dipole Components 6.6459 -3.7486 -0.3843
 Transition Dipole Components 1.4239 4.2191 -0.3270

Spin Up : Occ. MO --> Unocc. MO Coefficients

 57 --> 62 -0.386954
 55 --> 59 -0.465023

Spin Down: Occ. MO --> Unocc. MO Coefficients

 57 --> 62 0.386954
 55 --> 59 0.465023

27 (Transition) Excitation Energy 236.3 nm
 42319.7 1/cm

1 -> 28 Spin S 1.00
 State Dipole 6.2328
 Oscillator Strength 0.0000
 State Dipole Components 4.1044 -4.6888 -0.1284
 Transition Dipole Components 0.0000 0.0000 -0.0000

Spin Up : Occ. MO --> Unocc. MO Coefficients

 56 --> 61 0.434468
 55 --> 61 -0.462556

Spin Down: Occ. MO --> Unocc. MO Coefficients

 56 --> 61 0.434468
 55 --> 61 -0.462556

28 (Transition) Excitation Energy 219.3 nm
 45605.5 1/cm

1 -> 29 Spin S -0.00
 State Dipole 9.5707
 Oscillator Strength 0.0155
 State Dipole Components -1.9660 -9.3474 0.6004
 Transition Dipole Components 0.2013 0.8225 -0.0742

Spin Up : Occ. MO --> Unocc. MO Coefficients

 56 --> 60 0.460575
 55 --> 60 -0.455662

Spin Down: Occ. MO --> Unocc. MO Coefficients

	56	-->	60	-0.460575		
	55	-->	60	0.455662		
29 (Transition)	Excitation Energy			215.7 nm		
				46370.6 1/cm		
1 ->	30	Spin S	1.00			
		State Dipole	14.4936			
		Oscillator Strength	0.0000			
		State Dipole Components	-8.9709 -11.3125	1.2717		
		Transition Dipole Components	-0.0000 -0.0000	0.0000		
Spin Up : Occ. MO --> Unocc. MO Coefficients						

	55	-->	61	-0.411812		
Spin Down: Occ. MO --> Unocc. MO Coefficients						

	55	-->	61	-0.411812		
30 (Transition)	Excitation Energy			214.0 nm		
				46723.9 1/cm		
1 ->	31	Spin S	0.00			
		State Dipole	8.4550			
		Oscillator Strength	0.0926			
		State Dipole Components	-1.4807 -8.3087	0.5093		
		Transition Dipole Components	-1.9820 -0.4987	0.1963		
Spin Up : Occ. MO --> Unocc. MO Coefficients						

	56	-->	62	0.377585		
	55	-->	61	0.326276		
Spin Down: Occ. MO --> Unocc. MO Coefficients						

	56	-->	62	-0.377585		
	55	-->	61	-0.326276		
31 (Transition)	Excitation Energy			207.1 nm		
				48280.5 1/cm		
1 ->	32	Spin S	1.00			
		State Dipole	21.2254			
		Oscillator Strength	0.0000			
		State Dipole Components	10.5179 -18.4345	0.2475		
		Transition Dipole Components	0.0000 -0.0000	0.0000		
Spin Up : Occ. MO --> Unocc. MO Coefficients						

	54	-->	59	0.388435		
	54	-->	60	-0.580129		
Spin Down: Occ. MO --> Unocc. MO Coefficients						

	54	-->	59		0.388435	
	54	-->	60		-0.580129	
32 (Transition)	Excitation Energy			207.0 nm		
				48301.1 1/cm		
1 ->	33	Spin S		0.00		
		State Dipole		21.3257		
		Oscillator Strength		0.0001		
		State Dipole Components	10.6679	-18.4643	0.2324	
		Transition Dipole Components	-0.0079	-0.0753	0.0270	
Spin Up : Occ. MO --> Unocc. MO Coefficients						

	54	-->	59		0.388869	
	54	-->	60		-0.583079	
Spin Down: Occ. MO --> Unocc. MO Coefficients						

	54	-->	59		-0.388869	
	54	-->	60		0.583079	
33 (Transition)	Excitation Energy			205.5 nm		
				48650.1 1/cm		
1 ->	34	Spin S		1.00		
		State Dipole		19.3534		
		Oscillator Strength		0.0000		
		State Dipole Components	-11.3972	-15.5518	1.6724	
		Transition Dipole Components	-0.0000	-0.0000	0.0000	
Spin Up : Occ. MO --> Unocc. MO Coefficients						

	56	-->	60		0.434429	
Spin Down: Occ. MO --> Unocc. MO Coefficients						

	56	-->	60		0.434429	
34 (Transition)	Excitation Energy			204.7 nm		
				48862.5 1/cm		
1 ->	35	Spin S		0.00		
		State Dipole		16.0128		
		Oscillator Strength		0.0199		
		State Dipole Components	-8.1162	-13.7405	1.3167	
		Transition Dipole Components	0.4336	0.8199	-0.0645	
Spin Up : Occ. MO --> Unocc. MO Coefficients						

	56	-->	60		0.368854	
	55	-->	60		0.457856	

Spin Down: Occ. MO --> Unocc. MO Coefficients						

	56	-->	60		-0.368854	
	55	-->	60		-0.457856	
35 (Transition)	Excitation Energy			204.2 nm		
				48961.4 1/cm		
1 ->	36	Spin S		1.00		
		State Dipole		13.5926		
		Oscillator Strength		0.0000		
		State Dipole Components		-8.1714	10.8613	0.1357
		Transition Dipole Components		-0.0000	-0.0000	0.0000
Spin Up : Occ. MO --> Unocc. MO Coefficients						

	53	-->	59		-0.633303	
Spin Down: Occ. MO --> Unocc. MO Coefficients						

	53	-->	59		-0.633303	
36 (Transition)	Excitation Energy			204.1 nm		
				48994.1 1/cm		
1 ->	37	Spin S		0.00		
		State Dipole		13.5959		
		Oscillator Strength		0.0005		
		State Dipole Components		-8.2300	10.8211	0.1413
		Transition Dipole Components		-0.0021	-0.0107	0.1474
Spin Up : Occ. MO --> Unocc. MO Coefficients						

	53	-->	59		0.633182	
Spin Down: Occ. MO --> Unocc. MO Coefficients						

	53	-->	59		-0.633182	
37 (Transition)	Excitation Energy			203.7 nm		
				49099.5 1/cm		
1 ->	38	Spin S		1.00		
		State Dipole		23.0075		
		Oscillator Strength		0.0000		
		State Dipole Components		22.5019	4.3204	-2.0843
		Transition Dipole Components		-0.0000	-0.0000	0.0000
Spin Up : Occ. MO --> Unocc. MO Coefficients						

	55	-->	62		-0.586248	

Spin Down: Occ. MO --> Unocc. MO Coefficients				

	55	-->	62	-0.586248
38 (Transition)	Excitation Energy		198.5 nm	
			50381.1 1/cm	
1 ->	39	Spin S	0.00	
		State Dipole	6.9082	
		Oscillator Strength	0.0530	
		State Dipole Components	2.3015	-6.5126 0.1136
		Transition Dipole Components	-0.6520	1.3455 -0.0007
Spin Up : Occ. MO --> Unocc. MO Coefficients				

	56	-->	61	-0.562009
Spin Down: Occ. MO --> Unocc. MO Coefficients				

	56	-->	61	0.562009
39 (Transition)	Excitation Energy		188.6 nm	
			53030.3 1/cm	
1 ->	40	Spin S	0.00	
		State Dipole	8.2867	
		Oscillator Strength	0.8893	
		State Dipole Components	7.6692	-3.0995 -0.4959
		Transition Dipole Components	3.1292	-5.0864 0.0025
Spin Up : Occ. MO --> Unocc. MO Coefficients				

	56	-->	62	-0.398695
	55	-->	61	0.517145
Spin Down: Occ. MO --> Unocc. MO Coefficients				

	56	-->	62	0.398695
	55	-->	61	-0.517145
40 (Transition)	Excitation Energy		187.6 nm	
			53305.9 1/cm	
1 ->	41	Spin S	1.00	
		State Dipole	20.8411	
		Oscillator Strength	0.0000	
		State Dipole Components	17.8939	-10.6575 -0.7593
		Transition Dipole Components	-0.0000	0.0000 0.0000

Spin Up :	Occ. MO	-->	Unocc. MO	Coefficients

	54	-->	61	-0.659549

Spin Down:	Occ. MO	-->	Unocc. MO	Coefficients

	54	-->	61	-0.659549

41 (Transition) Excitation Energy 187.4 nm
53348.7 1/cm

1 -> 42 Spin S -0.00
State Dipole 20.6984
Oscillator Strength 0.0095

State Dipole Components 17.7682 -10.5898 -0.7574
Transition Dipole Components -0.3396 0.5116 0.0305

Spin Up :	Occ. MO	-->	Unocc. MO	Coefficients

	54	-->	61	0.657516

Spin Down:	Occ. MO	-->	Unocc. MO	Coefficients

	54	-->	61	-0.657516

42 (Transition) Excitation Energy 183.5 nm
54494.3 1/cm

1 -> 43 Spin S -0.00
State Dipole 15.8948
Oscillator Strength 0.3150
State Dipole Components 15.7803 1.3068 -1.3849
Transition Dipole Components 2.5612 2.3736 -0.3120

Spin Up :	Occ. MO	-->	Unocc. MO	Coefficients

	55	-->	62	-0.604705

Spin Down:	Occ. MO	-->	Unocc. MO	Coefficients

	55	-->	62	0.604705

43 (Transition) Excitation Energy 182.3 nm
54862.6 1/cm

1 -> 44 Spin S 1.00
State Dipole 14.0025
Oscillator Strength 0.0000
State Dipole Components -8.7520 10.9288 0.1856
Transition Dipole Components 0.0000 0.0000 -0.0000

Spin Up :	Occ. MO	-->	Unocc. MO	Coefficients		
	53	-->	60	0.365687		
	53	-->	62	0.477004		

Spin Down:	Occ. MO	-->	Unocc. MO	Coefficients		
	53	-->	60	0.365687		
	53	-->	62	0.477004		

44 (Transition) Excitation Energy 181.6 nm
55069.3 1/cm

1 -> 45 Spin S -0.00
State Dipole 14.0987
Oscillator Strength 0.0002
State Dipole Components -9.4458 10.4633 0.2638
Transition Dipole Components -0.0602 -0.0619 0.0354

Spin Up :	Occ. MO	-->	Unocc. MO	Coefficients		
	53	-->	60	0.391470		
	53	-->	62	0.466529		

Spin Down:	Occ. MO	-->	Unocc. MO	Coefficients		
	53	-->	60	-0.391470		
	53	-->	62	-0.466529		

45 (Transition) Excitation Energy 175.2 nm
57087.2 1/cm

1 -> 46 Spin S 1.00
State Dipole 15.4054
Oscillator Strength 0.0000
State Dipole Components -10.1556 11.5810 0.2650
Transition Dipole Components -0.0000 -0.0000 0.0000

Spin Up :	Occ. MO	-->	Unocc. MO	Coefficients		
	53	-->	60	0.538937		

Spin Down:	Occ. MO	-->	Unocc. MO	Coefficients		
	53	-->	60	0.538937		

46 (Transition) Excitation Energy 175.0 nm
57129.5 1/cm

1 -> 47 Spin S 0.00
State Dipole 15.2057

		Oscillator Strength	0.0000		
		State Dipole Components	-9.3939	11.9555	0.1841
		Transition Dipole Components	0.0056	0.0073	-0.0246
Spin Up : Occ. MO --> Unocc. MO Coefficients					

		53 -->	60	0.522332	
		53 -->	62	-0.331347	
Spin Down: Occ. MO --> Unocc. MO Coefficients					

		53 -->	60	-0.522332	
		53 -->	62	0.331347	
47 (Transition) Excitation Energy					
			173.0 nm		
			57794.0 1/cm		
1 ->	48	Spin S	1.00		
		State Dipole	27.3586		
		Oscillator Strength	0.0000		
		State Dipole Components	25.8827	-8.7344	-1.5127
		Transition Dipole Components	0.0000	0.0000	0.0000
Spin Up : Occ. MO --> Unocc. MO Coefficients					

		54 -->	62	-0.661222	
Spin Down: Occ. MO --> Unocc. MO Coefficients					

		54 -->	62	-0.661222	
48 (Transition) Excitation Energy					
			172.9 nm		
			57852.5 1/cm		
1 ->	49	Spin S	-0.00		
		State Dipole	27.3786		
		Oscillator Strength	0.0002		
		State Dipole Components	25.9117	-8.7103	-1.5169
		Transition Dipole Components	0.0637	-0.0096	0.0495
Spin Up : Occ. MO --> Unocc. MO Coefficients					

		54 -->	62	0.662286	
Spin Down: Occ. MO --> Unocc. MO Coefficients					

		54 -->	62	-0.662286	
49 (Transition) Excitation Energy					
			165.7 nm		
			60344.6 1/cm		
1 ->	50	Spin S	1.00		

State Dipole	15.2113		
Oscillator Strength	0.0000		
State Dipole Components	-9.6315	11.7717	0.2130
Transition Dipole Components	-0.0000	0.0000	-0.0000

Spin Up :	Occ. MO	-->	Unocc. MO	Coefficients

	53	-->	61	0.574034
	53	-->	62	-0.354528

Spin Down:	Occ. MO	-->	Unocc. MO	Coefficients

	53	-->	61	0.574034
	53	-->	62	-0.354528

50 (Transition) Excitation Energy	165.7 nm
	60361.8 1/cm

1 -> 51 Spin S	-0.00		
State Dipole	15.1931		
Oscillator Strength	0.0003		
State Dipole Components	-9.5438	11.8197	0.2032
Transition Dipole Components	-0.0183	0.0124	-0.0975

Spin Up :	Occ. MO	-->	Unocc. MO	Coefficients

	53	-->	61	-0.572243
	53	-->	62	0.358315

Spin Down:	Occ. MO	-->	Unocc. MO	Coefficients

	53	-->	61	0.572243
	53	-->	62	-0.358315

Energy=-18421.610035 Gradient=193.849191 Symmetry=C1

ENERGIES AND GRADIENT

Total Energy	=	-102375.0617709 (kcal/mol)
Total Energy	=	-163.141788254 (a.u.)
Binding Energy	=	-18421.6100351 (kcal/mol)
Isolated Atomic Energy	=	-83953.4517358 (kcal/mol)
Electronic Energy	=	-584860.5621504 (kcal/mol)
Core-Core Interaction	=	482485.5003795 (kcal/mol)
CI Energy	=	0.0000000 (kcal/mol)
Number of Configurations Used	=	51
Heat of Formation	=	-14053.8400351 (kcal/mol)
Gradient of Reference Configuration	=	193.8491915 (kcal/mol/Ang)

MOLECULAR POINT GROUP
C1

EIGENVALUES OF THE REFERENCE CONFIGURATION(eV)

Symmetry:	1 A	2 A	3 A	4 A	5 A
Eigenvalue:	-61.304966	-52.479424	-50.443546	-48.529068	-46.769363
Symmetry:	6 A	7 A	8 A	9 A	10 A
Eigenvalue:	-43.962723	-42.119900	-41.014301	-39.410393	-36.170040
Symmetry:	11 A	12 A	13 A	14 A	15 A
Eigenvalue:	-35.181664	-34.990940	-34.122169	33.514561	-32.144753
Symmetry:	16 A	17 A	18 A	19 A	20 A
Eigenvalue:	-31.727345	-28.930212	-28.754284	-27.197771	-26.182789
Symmetry:	21 A	22 A	23 A	24 A	25 A
Eigenvalue:	-25.654743	-25.010000	-24.148544	-23.823021	-23.179008
Symmetry:	26 A	27 A	28 A	29 A	30 A
Eigenvalue:	-22.414204	-21.763659	-21.558001	-21.547756	-21.000868
Symmetry:	31 A	32 A	33 A	34 A	35 A
Eigenvalue:	-20.089334	-19.912460	-19.750763	-19.550419	-19.036018
Symmetry:	36 A	37 A	38 A	39 A	40 A
Eigenvalue:	-18.887974	-18.579193	-18.282911	-18.049023	-17.722288
Symmetry:	41 A	42 A	43 A	44 A	45 A
Eigenvalue:	-17.287371	-17.138041	-16.799072	-16.490490	-16.176798
Symmetry:	46 A	47 A	48 A	49 A	50 A
Eigenvalue:	-16.038591	-15.517140	-15.280633	-14.754498	-14.682483
Symmetry:	51 A	52 A	53 A	54 A	55 A
Eigenvalue:	-14.012991	-13.352755	-12.686942	-12.527109	-12.019317
Symmetry:	56 A	57 A	58 A	59 A	60 A
Eigenvalue:	-11.868505	-10.278853	-4.492475	-3.780133	-3.269904
Symmetry:	61 A	62 A	63 A	64 A	65 A
Eigenvalue:	-2.585544	-2.333029	-1.800455	-0.929585	-0.861136
Symmetry:	66 A	67 A	68 A	69 A	70 A
Eigenvalue:	-0.818001	-0.617029	-0.336741	-0.185313	-0.134149
Symmetry:	71 A	72 A	73 A	74 A	75 A
Eigenvalue:	0.123394	0.361328	0.492120	0.779032	0.911911
Symmetry:	76 A	77 A	78 A	79 A	80 A
Eigenvalue:	0.960716	1.217651	1.732971	1.911359	2.218365

Symmetry:	81 A	82 A	83 A	84 A	85 A
Eigenvalue:	2.520534	2.725586	2.900362	3.258740	3.402930
Symmetry:	86 A	87 A	88 A	89 A	90 A
Eigenvalue:	3.424565	3.520794	3.631697	3.783182	4.317157
Symmetry:	91 A	92 A	93 A	94 A	95 A
Eigenvalue:	4.870071	4.940001	5.313831	5.576722	6.262230
Symmetry:	96 A	97 A	98 A	99 A	100 A
Eigenvalue:	6.502975	7.078451	7.735449	7.908369	8.120407
Symmetry:	101 A	102 A	103 A	104 A	105 A
Eigenvalue:	8.380394	8.749744	9.291595	9.571287	9.823945
Symmetry:	106 A	107 A	108 A		
Eigenvalue:	10.694991	11.597894	12.382694		

ATOMIC ORBITAL ELECTRON POPULATIONS

AO:	1	S	C	1	Px	C	1	Py	C	1	Pz	C	2	S	C
			1.087656			0.965193			0.993249			0.944930			1.086817
AO:	2	Px	C	2	Py	C	2	Pz	C	3	S	C	3	Px	C
			1.002989			0.951856			0.955206			1.089776			0.979939
AO:	3	Py	C	3	Pz	C	4	S	C	4	Px	C	4	Py	C
			0.947242			1.025247			1.089561			0.953653			0.986437
AO:	4	Pz	C	5	S	C	5	Px	C	5	Py	C	5	Pz	C
			0.983483			1.041129			0.970483			0.970604			0.995842
AO:	6	S	C	6	Px	C	6	Py	C	6	Pz	C	7	S	C
			1.001910			0.895936			0.974286			1.056477			1.097265
AO:	7	Px	C	7	Py	C	7	Pz	C	8	S	C	8	Px	C
			0.987476			0.958340			0.933955			1.018870			0.961122
AO:	8	Py	C	8	Pz	C	9	S	C	9	Px	C	9	Py	C
			0.964486			1.022468			1.000525			0.975255			0.894684
AO:	9	Pz	C	10	S	N	10	Px	N	10	Py	N	10	Pz	N
			1.088962			1.136932			1.140653			1.204970			1.452780
AO:	1	S	C	11	Px	C	11	Py	C	11	Pz	C	12	S	C
			0.938071			0.855342			0.865895			1.072333			1.006718
AO:	12	Px	C	12	Py	C	12	Pz	C	13	S	N	13	Px	N
			0.964790			0.917233			1.037779			1.129607			1.157358
AO:	13	Py	N	13	Pz	N	14	S	C	14	Px	C	14	Py	C

			1.197652		1.439499		1.051801		0.879992		0.979822
AO:	14	Pz C	15	S C	15	Px C	15	Py C	15	Pz C	
			1.032817		1.088056		0.951668		0.992558		0.962023
AO:	16	S C	16	Px C	16	Py C	16	Pz C	17	S C	
			1.089164		0.989430		0.966958		0.933747		1.084412
AO:	17	Px C	17	Py C	17	Pz C	18	S N	18	Px N	
			0.986630		0.942439		0.994670		1.201977		1.843275
AO:	18	Py N	18	Pz N	19	S C	19	Px C	19	Py C	
			1.186456		1.097931		1.051513		0.995897		0.971977
AO:	19	Pz C	20	S C	20	Px C	20	Py C	20	Pz C	
			0.899618		1.051176		0.989065		0.985906		0.893726
AO:	30	S C	30	Px C	30	Py C	30	Pz C	31	S O	
			1.006426		0.864561		0.930418		0.712003		1.692722
AO:	31	Px O	31	Py O	31	Pz O	33	S O	33	Px O	
			1.229178		1.503841		1.884758		1.809625		1.957204
AO:	33	Py O	33	Pz O	24	S H	25	S H	26	S H	
			1.292002		1.488986		0.951177		0.968058		0.959111
AO:	27	S H	28	S H	29	S H	21	S H	22	S H	
			0.955726		0.950784		0.932402		0.946136		0.946005
AO:	32	S H	23	S H	34	S H	35	S H	36	S H	
			0.751575		0.946194		0.979248		0.967174		0.981319
AO:	37	S H	38	S H	39	S H					
			0.966679		0.982458		0.978607				

NET CHARGES AND COORDINATES

Atom	Z	Charge	Coordinates(Angstrom)			Mass
			x	y	z	
1	6	0.008971	-0.28319	0.19238	0.38131	12.01100
2	6	0.003132	0.90546	-0.52107	0.31875	12.01100
3	6	-0.042204	2.10560	0.17493	0.19087	12.01100
4	6	-0.013133	-0.23172	1.58206	0.31306	12.01100
5	6	0.021942	0.96971	2.29716	0.18373	12.01100
6	6	0.071391	2.19327	1.57667	0.12118	12.01100
7	6	0.022964	2.26143	4.30176	-0.02417	12.01100
8	6	0.033054	1.00738	3.70463	0.11197	12.01100
9	6	0.040574	3.35802	3.45212	-0.06948	12.01100
10	7	0.064665	3.30535	2.18957	0.00241	14.00700
11	6	0.268358	4.51695	1.80238	-0.07110	12.01100

12	6	0.073480	4.68785	3.83609	-0.20042	12.01100
13	7	0.075883	5.33944	2.75786	-0.19329	14.00700
14	6	0.055569	6.60030	2.75400	-0.29637	12.01100
15	6	0.005695	7.34125	3.93420	-0.42431	12.01100
16	6	0.020701	6.65285	5.14944	-0.43645	12.01100
17	6	-0.008150	5.26229	5.10117	-0.31867	12.01100
18	7	-0.329639	4.95853	0.52275	-0.02124	14.00700
19	6	0.080996	5.14621	-0.18436	-1.28484	12.01100
20	6	0.080128	5.36307	-0.00549	1.27896	12.01100
30	6	0.486591	-0.07047	4.53970	0.16051	12.01100
31	8	-0.310499	-1.34167	4.16131	0.28748	15.99900
33	8	-0.547817	0.08117	5.73871	0.08950	15.99900
24	1	0.048823	7.14732	1.79655	-0.28679	1.00800
25	1	0.031942	2.97923	-0.48397	0.14590	1.00800
26	1	0.040889	0.89267	-1.62370	0.36696	1.00800
27	1	0.044274	-1.24683	-0.33624	0.47980	1.00800
28	1	0.049216	-1.21544	2.06247	0.36609	1.00800
29	1	0.067598	2.41183	5.39142	-0.09358	1.00800
21	1	0.053864	4.66146	6.02533	-0.32149	1.00800
22	1	0.053995	7.18644	6.10972	-0.53521	1.00800
32	1	0.248425	-1.87268	4.97563	0.29385	1.00800
23	1	0.053806	8.44040	3.90790	-0.51340	1.00800
34	1	0.020752	6.10517	0.12465	-1.75852	1.00800
35	1	0.032826	5.17587	-1.28462	-1.11800	1.00800
36	1	0.018681	4.31198	0.03213	-1.99089	1.00800
37	1	0.033321	5.70673	-1.06024	1.18794	1.00800
38	1	0.017542	6.20144	0.59357	1.70138	1.00800
39	1	0.021393	4.51163	0.02323	1.99626	1.00800

Dipole (Debyes)	x	y	z	Total
Point-Chg.	6.955	-3.043	-0.436	7.604
sp Hybrid	0.308	0.092	-0.033	0.323
pd Hybrid	0.000	0.000	0.000	0.000
Sum	7.263	-2.951	-0.469	7.854

HyperChem log stop -- Mon Jul 01 20:44:27 2002.